A Very Simple BICM-ID with EXIT Constraints

By Kisho Fukawa

A thesis submitted to
School of Information Science,
Japan Advanced Institute of Science and Technology,
in partial fulfilment of the requirements
for the degree of
Master of Information Science
Graduate Program in Information Science

Written under the supervision of
Professor Tad Matsumoto

March, 2011

A Very Simple BICM-ID with EXIT Constraints

By Kisho Fukawa (0910052)

A thesis submitted to
School of Information Science,
Japan Advanced Institute of Science and Technology,
in partial fulfilment of the requirements
for the degree of
Master of Information Science
Graduate Program in Information Science

Written under the supervision of
Professor Tad Matsumoto

and approved by
Professor Tad Matsumoto
Professor Yasushi Hibino
Professor Mineo Kaneko

February, 2011 (Submitted)

I certify that I have prepared this master thesis on my own without any inadmissible outside help.

JAIST, February 8, 2011

(Kisho Fukawa)

Author: _____

Date: _____

Supervisor: _____

Abstract

Bit-Interleaved Coded Modulation with Iterative Detection/Decoding (BICM-ID) has been recognized as being a bandwidth efficient coded modulation and transmission scheme. D. Zhao et al. proposed a yet very simple, close Shannon-limit achieving BICM-ID system. It uses very simple codes, irregular repetition and single parity check codes, combined with Extended Mapping (EM). With this structure, turbo cliff happens at a value of Signal-to-Noise power Ratio (SNR) around 1.5 dB to the Shannon limit. Even having known that the key role played towards the optimal design of the proposed code requires optimal degree allocation for variable nodes, in the original technique described above, though, the irregular allocation to the node degrees were determined only empirically. Another fundamental drawback of the original technique is that it still suffers from error floor. This is simply because the demapper EXtrinsic Information Transfer (EXIT) curve does not reach the top-right $(1.0, 1.0)$ Mutual Information (MI) point.

This thesis shows that the problem of the optimal degree allocation for the proposed BICM-ID technique can be solved by using Linear Programming (LP). Furthermore, this thesis introduces the use of partial accumulator, combined with the original system. With this technique, the right-most point of the demapper curve can be lifted up to which the point close enough to the (1.0,1.0) MI point, and thereby the convergence tunnel opens until (1.0,1.0) MI point. Based on those two optimization techniques, this thesis further investigates a technique to identify optimal labelling pattern for EM, so that the shape of the demapper EXIT curve can be flexibly changed.

This thesis introduces EXIT-constraint Binary Switching Algorithm (EBSA) and unbalanced labelling. It is shown through EXIT analysis that using EBSA and unbalanced labelling, demapper and decoder EXIT curves closely match, and thereby, it can achieve near-capacity performance. Simulation results for the proposed techniques are given in this thesis to verify that it can achieve near-Shannon limit performance. It is shown that using the proposed optimization techniques, threshold SNR is only 0.54 dB away from the Shannon limit even though its required complexity is very low; the complexity is at the same level as a turbo code with only memory-2 convolutional constituency codes.

Keywords: BICM-ID, Single Parity Check Code, Irregular Repetition Code, Extended Mapping, Optimization, Partial Accumulator, EXIT based Binary Switching Algorithm, Unbalanced Labelling.

Contents

List of Figures

List of Tables

Chapter 1

Introduction

Recently, wireless communications are widely used in our daily life. Examples are voice communications over cellular wireless networks, Internet connection via WiFi and etc. Those technologies are still developing towards an ultimate goal of human being, where people can communicate and access the necessary data anywhere at any time. One of the challenges is to develop a technological basis that allows for more data to be transmitted reliably over wireless communication systems at a time, so that high data rate transmission is made possible. Another emerging challenge is to realize energy efficient wireless communication systems to reduce carbon dioxide emission. Reduction of computational burden for communication system is obviously inevitable challenge. Those three challenges are related each other.

When Signal-to-Noise power Ratio (SNR) for the communication system is given, maximum code rate for channel coding which achieves arbitrary low Bit Error Rate (BER) can be derived. This theoretical limit in rate is called channel capacity; if the rate for channel coding is smaller than the channel capacity, arbitrary low BER can uniquely achieved. In addition, given the bit rate of the system, there exists a required SNR, and if it is larger than the threshold value, BER can be made arability small. This threshold in SNR is called "Shannon limit" [1]. Approaching this channel capacity and Shannon limit is the key element upon designing of wireless communication systems with high data transmission rate and high energy efficiency.

Bit-Interleaved Coded Modulation with Iterative Detection/Decoding (BICM-ID) [2] has been recognized as being a bandwidth efficient coded modulation and transmission scheme, of which transmitter is comprised of a concatenation of encoder and bit-to-symbol mapper separated by a bit interleaver. Iterative demapping-and-decoding takes place at the receiver, where *extrinsic* Log Likelihood Ratio (LLR) obtained as the result of the Maximum *A posteriori* Probability (MAP) algorithm for demapping/decoding is forwarded to the decoder/demapper via deinterleaver/interleaver, and used as the *a priori* LLR for decoding/demapping, according to the standard turbo principle. Performances of BICM-ID have to be evaluated in terms of convergence and asymptotic properties [3], which are represented by the threshold SNR

and BER floor, respectively. In principle, since BICM-ID is a serially concatenated system, analysing its performances can rely on the area property [4] of the EXtrinsic Information Transfer (EXIT) chart representing the Mutual Information (MI) exchange. Therefore, the transmission link design based on BICM-ID falls into the issue of matching between the demapper and decoder EXIT curves. Various efforts have been made, seeking for better matching between the two curves for minimizing the gap while still keeping the convergence tunnel open, aiming, without requiring heavy demapping/decoding complexity, at achieving lower threshold SNR and lower BER floor.

D. Zhao et.al. proposed a yet very simple, close Shannon-limit approaching BICM-ID system [5]. It uses very simple codes, irregular repetition and single parity check codes, combined with Extended Mapping (EM). There are two issues which must be solved to achieve the best performance with this technique. One is: even having known that the key role played towards the optimal design of the proposed code is the degree allocation for variable nodes, as shown in [5], though, the irregular degree allocation to the node degrees were determined only empirically. Another fundamental drawback of the previous work is that it still suffers from the error floor. This is simply because the demapper EXIT curve does not reach the top-right $(1.0, 1.0)$ MI point. This thesis proposes techniques to cope with those issues. It is shown in this thesis that obtaining the optimal degree allocation falls into the Linear Programming (LP) problem. Moreover, this thesis shows the technique to make the demapper curve reach the top-right $(1.0, 1.0)$ MI point by using partial accumulator. Further more, this thesis re-visits the issue of labelling pattern for the mapping. This is because with the partial accumulator, the labelling pattern used in the previous work should not necessarily be optimal. This thesis then introduces a new techniques, EXIT constraint Binary Switching Algorithm (EBSA) and unbalanced labelling. Simulation results are shown in this thesis to demonstrate the superiority of the proposed techniques. The results show that near-Shannon limit performance can be achieved with the proposed technique; BER simulation shows that the threshold SNR is only 0.54dB away from the Shannon limit with a code structure, of which complexity is at the same level as a turbo code with only memory-2 convolutional constituency codes.

This thesis is organized as follows: in **Chapter 2**, the system model is presented and the basics of the techniques investigated in this thesis are described. **Chapter 3** investigates the EXIT chart as a tool for analysing and optimizing iterative receivers. **Chapter 4** introduces the LP technique to obtain optimal degree allocation. **Chapter 4** presents a use of partial accumulator where it is described in detail that how it works and what effect it makes to the EXIT chart. **Chapter 6** introduces the EBSA and unbalanced labelling techniques for achieving optimal labelling pattern. **Chapter 7** shows the results from the simulations conducted to verify the effectiveness of the techniques proposed in this thesis. Finally conclusions are given in **Chapter 8**.

1.1 Research Contribution

By applying the technique proposed in this thesis achieves the near optimal performance of the original system while keeping the simple structure. It should be noted that complexity of the system is the same level as a turbo code with only memory-2 convolutional constituency codes, while proposed system can achieve almost the same performance as the optimal memory-4 convolutional constituency Turbo code.

Chapter 2

Introduction to BICM-ID

In this chapter, basics of the technique, BICM-ID, is introduced. The investigation starts from the general property of the communication system and their performance limit represented by Shannon-Limit. The BICM-ID system is then explained, covering from fundamental principle to the performance tendency/property of the technique. The detailed descriptions of Single Parity Check node assisted Irregular Repetition Coded BICM-ID with Extended Mapping are also provided, of which optimal design is the major objective of this thesis. Finally, in this chapter, performance evaluation result for BICM-ID without optimization is presented.

2.1 Information Source Model

In digital communications, various kinds of information has to be delivered to the destination via communication channels. The use of information source coding enable to digitalize the data into a bit stream. One of the well known information source coding technique is Huffman coding [6] which is optimal in the sense that it can achieve the shortest expected code length. However, information source coding is out of the scope of this thesis. In this thesis, no specific practical source is assumed and thereby, this thesis takes into account the source only in the abstract sense. It is assumed that information source is expressed in a binary form, 0 and 1, with their appearance probabilities being identical, i.e,

$$Pr(b = -1) = Pr(b = +1) = \frac{1}{2}, \tag{2.1}$$

where $Pr(b = -1)$ and $Pr(b = +1)$ denote the appearance probabilities of 1 and 0, respectively.

2.2 Channel Coding

Channel coding is used to protect the source information from the errors occurring while the binary data stream is transmitted via a noisy channel. Channel coding is performed by adding some redundancy to the source information. Code rate R describes the ratio of source-information-to-channel-coded sequence,

$$R = \frac{K}{K'}, \tag{2.2}$$

where K is the source information sequence length and K' is the channel-coded sequence length. The larger the redundancy due to channel coding, the higher the power efficiency if the channel is properly designed, but the lower the spectrum efficiency. Hence, given the spectrum efficiency of the system required, there exists a required threshold SNR and if the operational SNR is larger than the threshold value, Shannon's channel coding theorem [1] predicts that there exist a channel code with rate R such that BER can be made arability small. This threshold in SNR is called "Shannon limit". Using the redundancy added to the bit stream, detection and correction of errors occurring in the channel can be performed at the receiver side. This process is called decoding. Decoding also removes the redundancy added by encoding.

After the publication of Shannon's theorem, a lot of efforts have been made to find codes that can achieve the Shannon limit. Discovery of Turbo code, found by Berrow [7] in 1993, was a landmark event in the history of Information theory, since the code can asymptotically achieve the Shannon limit. It is shown in [7] that Turbo code comprised of memory-4 constituency convolutional codes can achieve 0.6 dB, in SNR, to the Shannon limit. Today, Turbo code is widely used in various applications, where the extrinsic information exchange plays key role towards designing limit achieving turbo code as stated in [7]. This fundamental mechanism is known as turbo principle, and it is also widely used to design Shannon limit approaching techniques based on the turbo principle.

2.3 Modulation

In wireless communications, modulation is a process of converting from bit stream to radio wave. In order to convey the bit stream, the carrier signal having a center frequency f_c has to change its properties according to the data format. In Quadrature Amplitude Modulation (QAM), the amplitude and phase of the single carrier signal centred at f_c simultaneously controlled, according to the data. Note that composition of amplitude modulated two carriers having the same center frequency with phase or 4-QAM shifted by $\pi/2$ can be seen as being equivalent to Quaternary Phase Shift-Keyed (QPSK) single carrier signal. As in many digital modulation schemes,

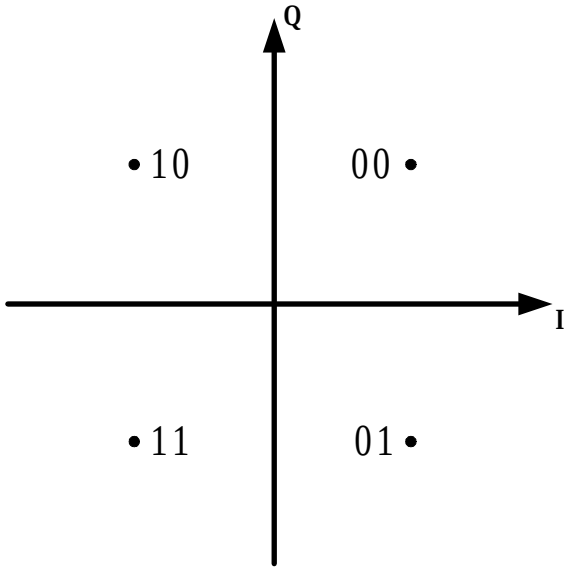

Figure 2.1: Gray Mapping for 4-QAM

the constellation diagram is a useful representation of the signal. With the 2^M-QAM constellation, amplitudes of the both In-phase and Quadrature components in the complex base-band signal expression change, if $M > 2$. The assigned signal points follow the constellation diagram, and labelling patterns are determined by the mapping rule. The process for recovering a bit stream from a received signal is called demapping.

Fig. 2.1 shows the labelling pattern of Gray-Mapped 4-QAM. The figure shows that 2 bits are assigned to one symbol and one symbol is assigned to one signal constellation point. In general, modulation scheme with 2^M constellation points yield M bits-per-symbol spectrum efficiency. Wireless communication systems before the turbo principle was introduced, relied only on the concept that mapping pattern is designed so that bit pattern pairs having larger Hamming distance is allocated to the signal points having larger Euclidean distance. Hamming distance refers to the number of unequal bits between the two bit-mapping patterns. The 4-QAM mapping pattern shown in Fig. 2.1, which is called Gray mapping, is designed so that the pair of two bit-mapping pattern havin maximum Hamming distance is placed as the two signal points having the maximum Euclidean distance. With this mapping rule, the symbol-wise detection error causes smallest number of bit errors, compared to other mapping rules. However, this is the case only if no *a priori* information is available. In the Section. 2.7.3, other mapping techniques which are better suited to BICM-ID using the turbo principle is explained.

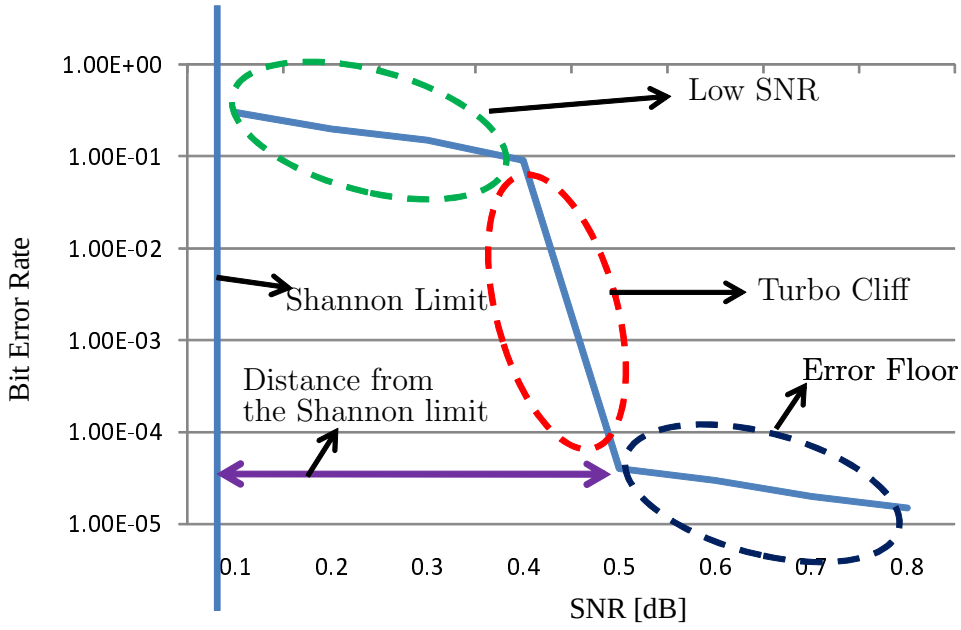

Figure 2.2: Bit-Error-Rate Chart and Shannon Limit

2.4 Channel Capacity

When SNR of a communication system is given, maximum channel coding code rate for achieving arbitrary low BER is uniquely determined. This is well known as the channel capacity C : i.e. if $R \leq C$, arbitrarily small BER can be achieved [1]. The channel capacity C of a communication system using Gaussian code book in Additive White Gaussian Noise (AWGN) channels is given by,

$$C = B \log(1 + SNR), \tag{2.3}$$

where B is the bandwidth of the system. Properties of AWGN are explained more in detail in Section 2.7.2. Approaching the channel capacity (or equivalently Shannon limit) is, therefore, the key to designing optimal wireless communication systems with high spectrum and power efficiencies. SNR represented in the liner domain can be converted into the logarithm domain by,

$$10 \log_{10}(SNR) \text{ dB}, \tag{2.4}$$

where in the logarithm domain, the unit is in decibel (dB). As described before, Shannon's theorem states that if $C \geq R$, arbitrary small BER can be achieved. Performance of Shannon limit approaching system can be evaluated by BER. Relationship between SNR and BER for Turbo codes or turbo systems following the turbo principle is illustrated in Fig. 2.2. As can be seen from the figure, shape of

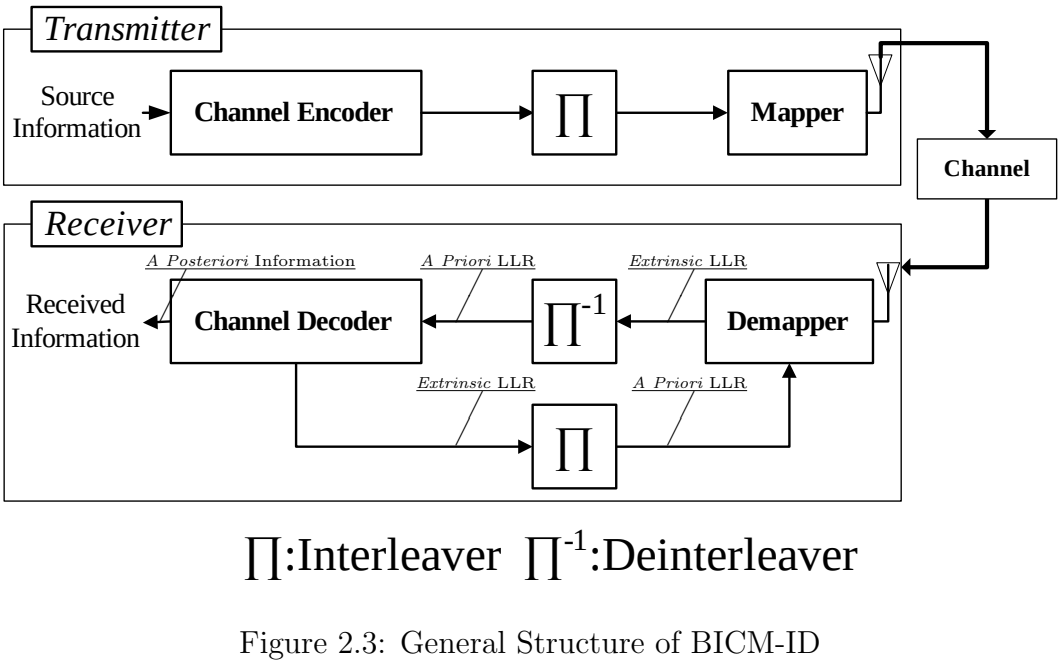

Figure 2.3: General Structure of BICM-ID

the BER curve is segmented into thee three categories, depending on SNR; one is high BER range corresponding to low SNR values; when SNR gradually increases, steep decrease of BER happens, which is called turbo cliff; after the turbo cliff, BER decrease may plateaus, which is referred to as BER floor. Note that turbo cliff is only observed when system following the turbo principle is used. Therefore, shifting the turbo cliff closer to the Shannon-limit enables to send and receive data with lower transmission power while assuring low BER. Note that the SNR point, where turbo cliff happens, depends not only on code rate but also "matching" of the components in the system. The "matching" can well be explained by the EXIT characteristic of the turbo system. This will be explained more in detail in Chapter 3.

2.5 BICM-ID in General

BICM-ID [2] has been recognized as being a bandwidth efficient coded modulation and transmission scheme, of which transmitter is comprised of a concatenation of encoder and bit-to-symbol mapper separated by a bit interleaver. General BICM-ID structure is diciped in Fig. 2.3. Iterative demapping (detecting) and decoding takes place at the receiver, which forms a turbo loop. Over the turbo loop, *extrinsic* LLR obtained as the result of the MAP algorithm for demapping/decoding is forwarded to the decoder/demapper via deinterleaver/interleaver, and used as the *a priori* LLR for decoding/demapping.

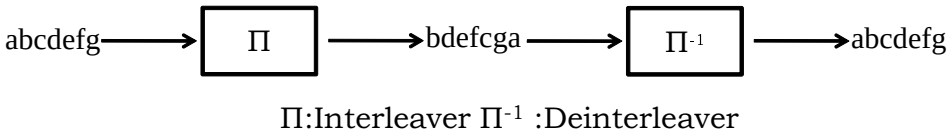

Figure 2.4: Interleaver and Deinterleaver

2.5.1 Interleaver and Deinterleaver

Interleaver permutates the order of the bits in the stream, while deinterleaver reorders the permutated bits. Conventional usage of interleaver/deinterleaver is to spread the burst errors caused in the channel, because majority of error correction codes is designed so that it can correct random errors. On the contrary, in the BICM-ID systems, interleaver and deinterleaver are used to obtain the randomness of the code itself, following the random coding concept which Shannon used when giving proof to the channel coding theorem. As a result, interleaving and deinterleaving reduce the correlation between the LLRs so that both demapping and decoding can performed independently without making any influence each other. Fig. 2.4 illustrates the roles of interleaver and deinterleaver, where bit stream is expressed in *alphabets* to clearly show how the interleaving and deinterleaving processes work.

2.5.2 LLR

LLR is defined as,

$$L(b_k) = \ln \frac{Pr(b_k = +1)}{Pr(b_k = -1)} \tag{2.5}$$

where $Pr(b_k = +1)$ and $Pr(b_k = -1)$ denote the probabilities of the kth channel coded bit being 0 and 1, respectively. For a given LLR value it is possible to calculate the probability that $b_k = +1$ or $b_k = -1$ by using

$$Pr(b_k = +1) = \frac{exp(L(b_k))}{1 + exp(L(b_k))} \tag{2.6}$$

$$Pr(b_k = -1) = \frac{1}{1 + exp(L(b_k))} \tag{2.7}$$

The LLR given by (2.5) is used as the *a priori* LLR in the systems following the turbo principle. The *a priori* LLR is the knowledge provided from the other components of the system. In BICM-ID, *a priori* information is fed back from the decoder/demapper to the demapper/decoder in the form of *extrinsic* information before the interleaver/deinterleaver.

2.6 Turbo Principle

In BICM-ID, LLR is exchanged between the demapper and the decoder, which forms so called "turbo loop". There are three types of LLR information used in the turbo loop; *a priori*, *extrinsic* and *a posteriori* LLRs. As mentioned in previous section, the *a priori* LLR is the knowledge provided from the other components of the system. *Extrinsic* LLR is the gain of the knowledge obtained by performing the processing for demapping/decoding using the *a priori* information provided by decoder/demapper. Demapper or decoder input and output correspond to *a priori* and *extrinsic* LLRs, respectively. Note that demapper/decoder *extrinsic* LLR is used as *a priori LLR* for decoder/demapper, according to the turbo principle. In BICM-ID, demapping is performed using received signal points and the *a priori* LLR from the decoder. However, in the first iteration, *a priori* LLR from the decoder is zero since decoding is not yet performed and no information is fed back from the decoder. After the processing for demapping is performed, the extrinsic LLR is obtained for each transmitted coded bit, which is then forwarded to the decoder via deinterleaver. The decoder uses the demapper output *extrinsic* LLR and performs decoding. This *extrinsic* LLR output from the decoder is then fed back to the demapper via interleaver, and used as the *a priori* LLR. This iterative process is repeated until no gain in mutual information is achieved by iterations. When iterative process is terminated, decoder makes the final decision that whether the bit is 0 or 1, based on the sign of *a posteriori* LLR, given by

$$a\ posteriori\ \text{LLR} = a\ priori\ \text{LLR} + extrinsic\ \text{LLR} \tag{2.8}$$

An illustrative example of this process is given in Fig. 2.3.

2.7 Single Parity Check Irregular Repetition Coded BICM-ID with Extended Mapping

D. Zhao et.al. proposes a yet very simple, close Shannon-limit approaching BICM-ID system [5]. It uses very simple codes, Single Parity Check Codes (SPCC) and Irregular Repetition Code (IRC), combined with 4-QAM Extended Mapping for modulation. Structure of this system is depicted in Fig. 2.5. First of all, the source information is channel-encoded using SPCC, followed by IRC encoding. After the channel encoding process, the encoded bit stream is interleaved and sent to the receiver with 4-QAM Extended Mapping (EM) modulation. Channel is assumed to be suffering from AWGN. At the receiver side, demapping of EM and decoding of SPCC and IRC take place iteratively following the turbo principle. For simplicity in notation, this technique is referred to as SPCCIRC-BICM-ID-EM. In following sections, roles to be played and algorithm performed in each component of the SPICCIRC-BICM-ID-EM are detailed.

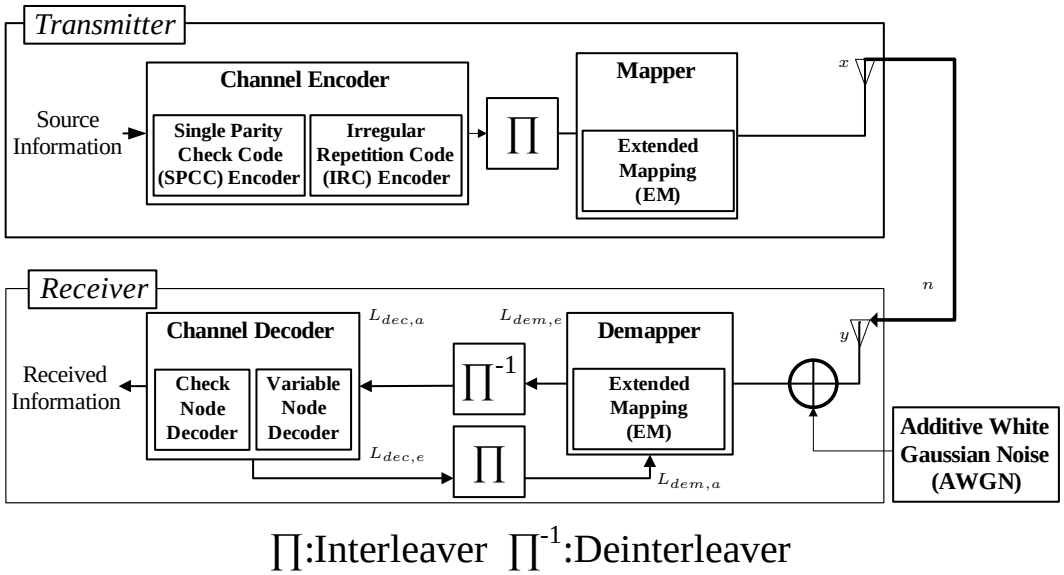

Figure 2.5: Single Parity Check Irregular Repetition Coded BICM-ID with Extended Mapping

2.7.1 Channel Coding

First of all, bit sequence $\boldsymbol{b}$ of the source information is encoded using the SPCCIRC-encoder. Here, Single Parity Check Code (SPCC) and Irregular Repetition Code (IRC) are used. SPCC encoding is the process where a single parity bit is added for every $d_c - 1$ information bits. d_c is referred to as check node degree. The SPCC encoder is followed by the IRC encoder. Fig. 2.6, shows an example of the SPCC encoding process. In the example shown in Fig. 2.6, $d_c = 7$. Following the SPCC,

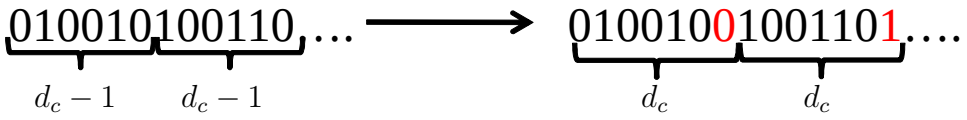

Figure 2.6: Example of Single Parity Check Code ($d_c = 7$).

IRC encoding is performed. The repetition times d_v, referred to as variable node degree, take different values in one whole block (=transmission frame); if d_v takes several different values in a block, such code is referred to as having irregular degree allocation. In the case of irregular degree allocation, the ratio of the blocks having the same d_{vi} value-to-the-total length of the block defines the degree distribution a_i. An example of IRC is given in Fig. 2.7. Here, $\{d_{v1}, d_{v2}\} = \{2, 3\}, \{a_1, a_2\} = \{0.6, 0.4\}$. The total code rate $R_{SPCCIRC}$ of the code can thus be expressed as

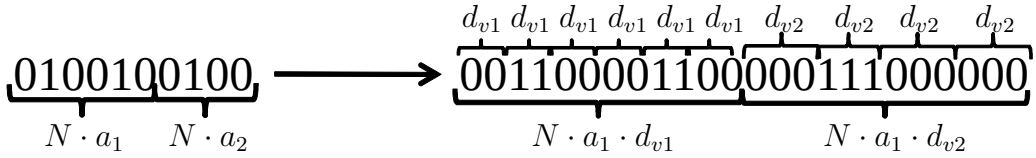

Figure 2.7: Example of Irregular Repetition Code ($N = 10$bits).

$$R_{IRCSPCC} = \frac{(d_c - 1)}{(d_c \cdot \sum_i a_i \cdot d_{v,i})} \tag{2.9}$$

Spectrum efficiency $R_{S,SPCCIRC}$ is given by

$$R_{S,SPCCIRC} = l_{map} \cdot R_{SPCCIRC} \tag{2.10}$$

$$= \frac{l_{map} \cdot (d_c - 1)}{(d_c \cdot \sum_i a_i \cdot d_{v,i})} \tag{2.11}$$

bits per symbol, where l_{map} denotes the bit length per symbol for mapping.

2.7.2 AWGN Channel

Before detailing the SPCCIRC-BICM-ID-EM scheme, explanation of the channel property is provided in this section. This is because performance of demapping is highly depending on the channel, and therefore having the knowledge about the channel property is a prerequisite for the understanding and analysing modulation techniques. This thesis assumes frequency flat AWGN channel. If the channel exhibits frequency selectivity due to the multipath propagation, the receiver needs an equalizer to eliminate the inter-symbol interference. However, combining SPCCIRC-BICM-ID-EM with the turbo equalization framework [8]-[9] is rather straightforward. It is assumed that transmission chain is properly normalized so that the received SNR $= 1/\sigma_n^2$; with this normalization, the channel complex gain term from the mathematical expression of the channel can be properly deleted. The discrete time description of the received signal $y(m)$ is then expressed by

$$y(m) = x(m) + n(m), \tag{2.12}$$

where, with m being the symbol timing index, $x(m)$ is the transmitted modulated signal with unit power, and $n(m)$ the zero mean complex AWGN component with variance σ_n^2 (i.e., $< |x(m)|^2 >= 1, < n(m) >= 0$, and $< |n(m)|^2 >= \sigma_n^2$).

2.7.3 Extended Mapping

After SPCCIRC encoding, the coded bit sequence is bit-interleaved with the interleaver, segmented into l_{map}-bit segments, and then the each segment is mapped on

to one of the 2^M constellation points for modulation. In SPCCIRC-BICM-ID-EM, $l_{map} > M$ because EM is assumed. With the EM technique, more than one labels having different bit patterns in the segment are mapped on to each constellation point. However, there are many possible combinations of bit patterns to be allocated to the constellation points. In the SPCCIRC-BICM-ID technique presented in [5] uses the labels assigned to the each constellation point, obtained by [10], so that, with full a priori information, the MI between the coded bit and the demapper output extrinsic LLR at the right most point of the demapper EXIT curve is maximized. Details about obtaining optimal labelling pattern is explained in Chapter 6. Fig. 2.8 shows the optimal labelling pattern for 4-QAM with $l_{map} = 5$ in the sence that the right most-point of the demapper EXIT curve has the largest MI. It should be noted here that the labelling pattern is equivalent to that obtained by compressing the 32-QAM constellation, as shown in Fig. 2.9. The complex-valued signal modulated according to the mapping rule, referred to as x, is finally transmitted to the wireless channel. The advantage of EM over high order-modulation such as 32-QAM, is that it is less sensitive to various impairments such as I-Q imbalance and/or phase jitter. Fig. 2.10 and Fig. 2.11 shows the EM 4-QAM and 32-QAM constellation points, respectively, suffering from AWGN. It can be clearly seen that 32-QAM constellation points has larger possibility of being demapped incorrectly. A Tanner graph representation of the transmitter is given in Fig. 2.12.

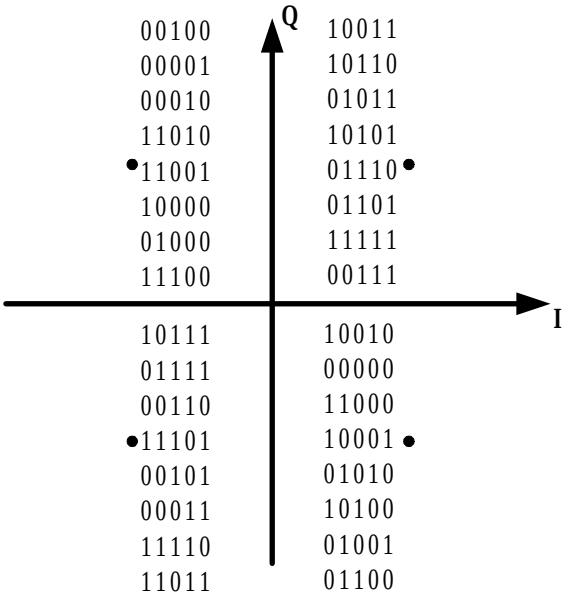

Figure 2.8: 4-QAM Extended Mapping

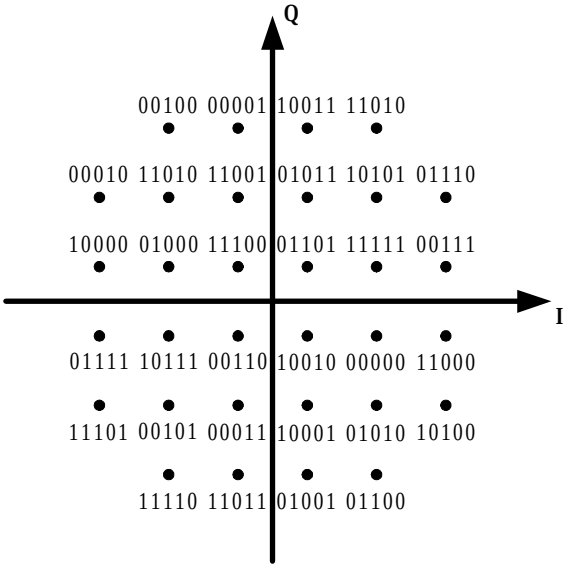

Figure 2.9: Optimized 32-QAM Labelling Pattern

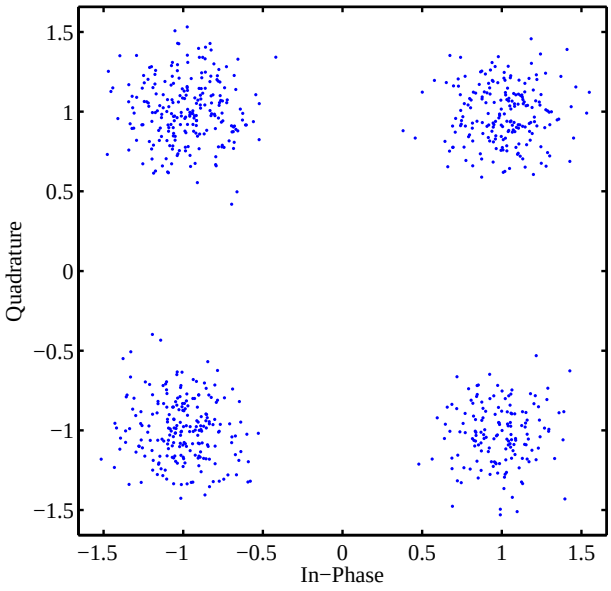

Figure 2.10: AWGN Noised 4-QAM

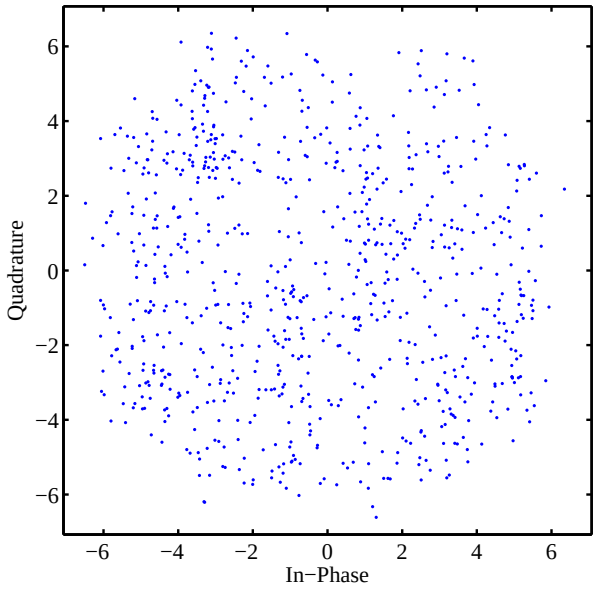

Figure 2.11: AWGN Noised 32-QAM

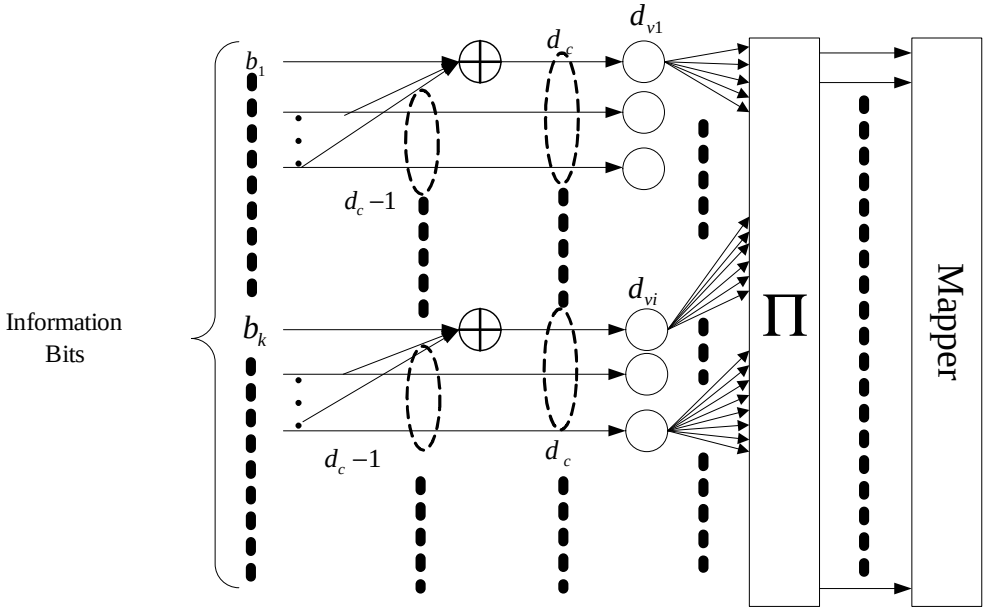

Figure 2.12: Tanner Graph of the Transmitter

2.7.4 Demapper

At the receiver side, the iterative processing is invoked, where extrinsic information is exchanged between the demapper and decoder. Using received signal sample $y(m)$ and the *a priori* LLR fed back from the decoder, *extrinsic* LLR of the νth bit in the labelling vector in the symbol transmitted at the mth symbol timing of the demapper can be expressed as,

$$L_{dem,e}(y(m)|b_\nu(m)) = \ln \frac{\sum_{v=1,v\neq\nu}^{l_{map}} Pr(y(m)|b_v(m)=+1)}{\sum_{v=1,v\neq\nu}^{l_{map}} Pr(y(m)|b_v(m)=-1)}, \tag{2.13}$$

where $Pr(y(m)|b_v(m)=+1)$ and $Pr(y(m)|b_v(m)=-1)$ denote the probability of $y(m)$, given the a priori information $b_v(m)$ conditioned upon the vth position of the bit-mapping pattern being 0 and 1. This can be further described as,

$$L_{dem,e}[b_\nu(m)] = \ln \frac{\sum_{s\in S_0} \exp\{-\frac{|y-s|^2}{\sigma_n^2}\} \prod_{v=1,v\neq\nu}^{l_{map}} exp(-b_v(s)L_{dem,a}(b_v(s))}{\sum_{s\in S_1} \exp\{-\frac{|y-s|^2}{\sigma_n^2}\} \prod_{v=1,v\neq\nu}^{l_{map}} exp(-b_v(s)L_{dem,a}(b_v(s))} \tag{2.14}$$

where s denotes a signal point in the constellation, $S_0(S_1)$ indicates the set of the labels having the νth bit being 0(1), and $L_{dem,a}(b_v(s))$ is the demapper's *a priori* LLR fed back from the decoder corresponding to the v^{th} position in the label allocated to the signal point s.

2.7.5 Decoder

Decoding takes place segment-wise where, because of the irregular code structure, the variable node degrees $d_{v,i}$ have different values segment-by-segment. Structure of the decoder is given in Fig. 2.13 The $d_{v,i}$ bits constituting one segment, output from

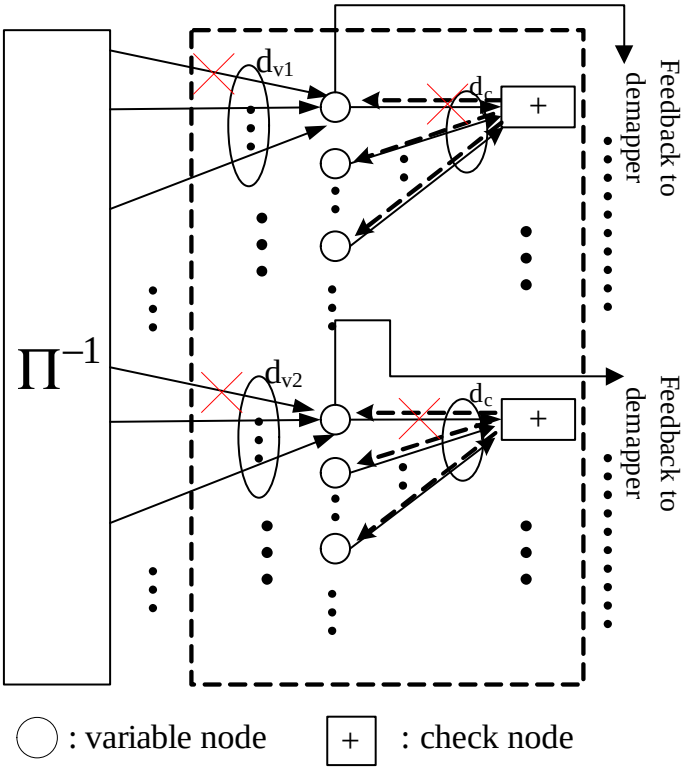

Figure 2.13: Decoder Structure

the de-interleaver, are connected to a variable node, and d_c variable nodes are further segmented and connected to a check node decoder; those demapper output bits in one segment, connected to the same variable node decoder, are not overlapping with other segments, and so is the case of the variable node segmentation. Therefore, no iterations in the decoder are required. The extrinsic LLR update for a bit at the check node is exactly the same as the check node operation in the LDPC codes, as

$$L_{cnd,e,\nu} = \sum_{u=1,u\neq\nu}^{d_c} \boxplus L_{dec,a,u} \tag{2.15}$$

$$= 2\arctan\Big(\prod_{u=1,u\neq\nu}^{d_c} \tanh(L_{dec,a,u}/2)\Big) \tag{2.16}$$

where $\boxplus$ is referred to as the box-sum operator [3], and $L_{cnd,a,u} = L_{dem,e,u}$ is the *a priori* LLR for the uth bit in the νth segment. The it extrinsic LLR, calculated by the check node decoder, is fed back to its connected variable node decoder, where it is further combined with $(d_{v,i} - 1)$ *a priori* LLRs forwarded from the demapper via the deinterleaver, as

$$L_{dec,e,\nu'} = L_{cnd,e,\nu} + \sum_{q=1,q\neq\nu'}^{d_{v,q}} L_{cnd,e,q} \tag{2.17}$$

This process is performed for the other bits in the same segment, and also for all the other segments independently in the same transmission block. Finally, the updated *extrinsic* LLRs obtained at the each variable node are interleaved, and fed back to the demapper. For the final bit decision, *a posteriori* output of the decoder is used. A Tanner graph representation of the receiver is depicted in Fig. 2.14.

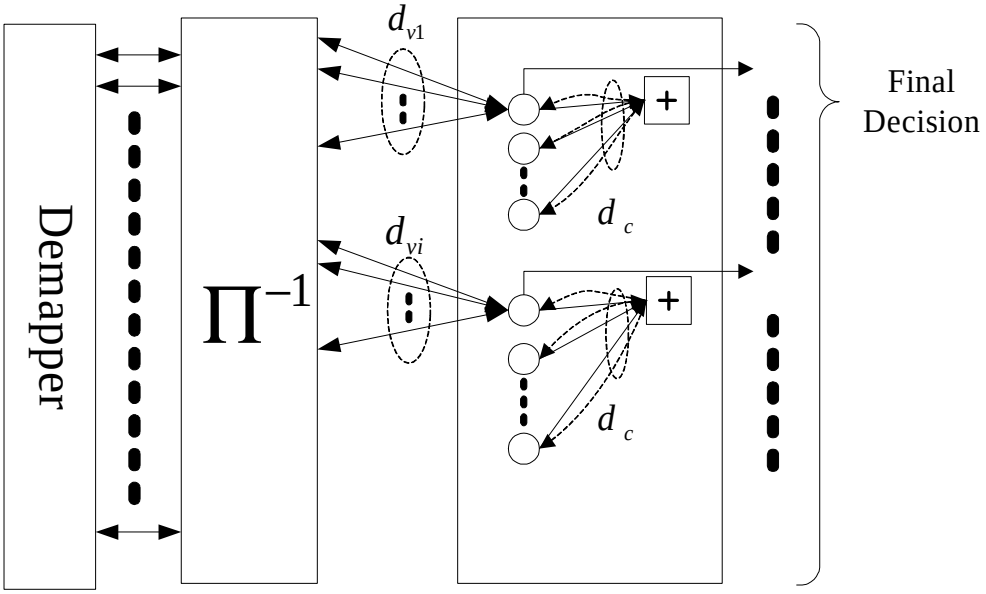

Figure 2.14: Tanner Graph of the Receiver

2.7.6 Bit-Error-Rate Performance Analysis

BER performance of the original technique presented in [5] was evaluated via benchmark simulations. The result is shown in Fig. 2.15 for $d_c = 80, \{d_{v1}, d_{v2}\} = \{5, 7\}, a = \{a_1, a_2\} = \{0.77, 0.23\}$ and $d_c = 100, \{d_{v1}, d_{v2}\} = \{3, 5, 6\}, \{a_1, a_2, a_3\} = \{0.58, 0.41, 0.01\}$. Note that the node degrees and node degree allocations are exactly the same as that used in [5], which were obtained empirically so that the BER threshold happens at a SNR point as close to the Shannon limit as possible. From Fig. 2.15, it can be

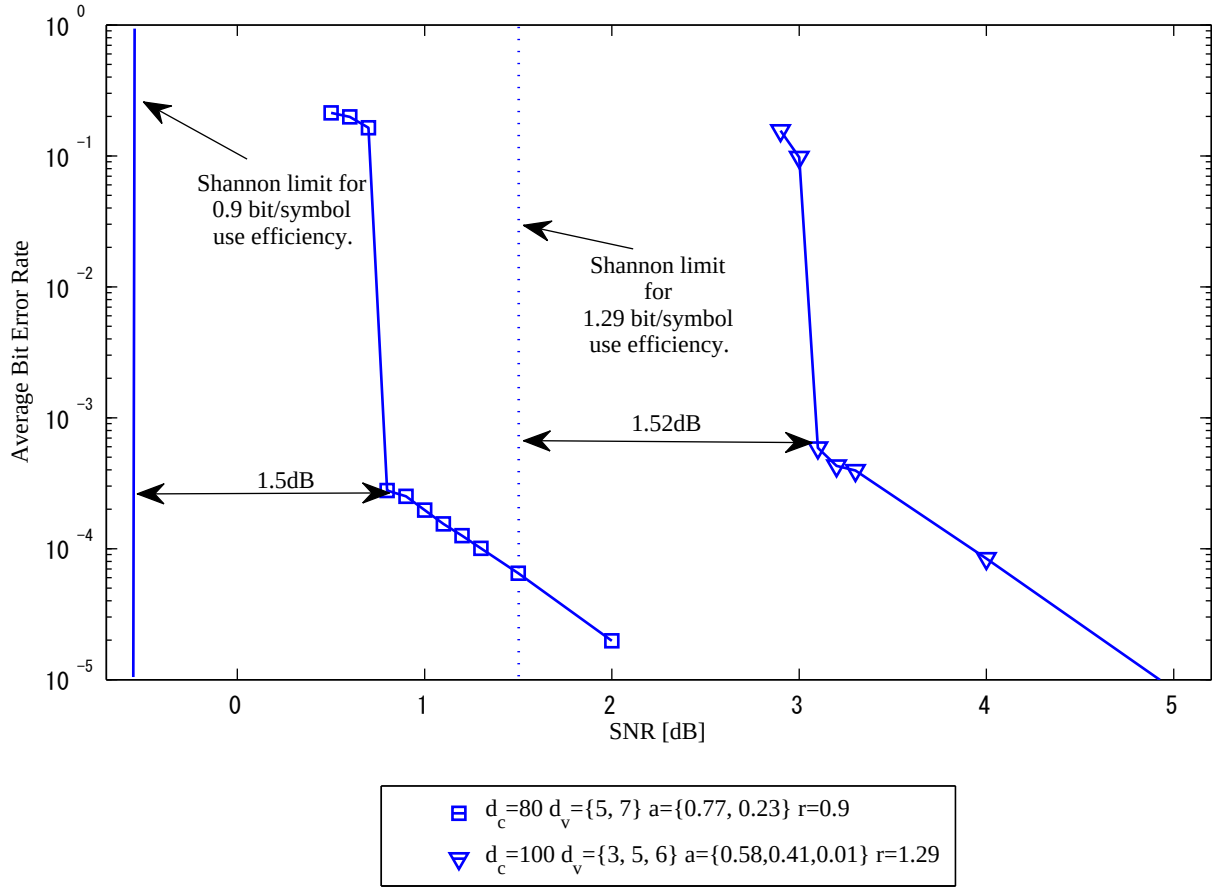

Figure 2.15: BER Chart: SPCCIRC-BICM-ID-EM

observed that for the both BER curves clear turbo cliff happen. It should be noted here that the BER curves are exactly consistent to those shown in [5]. As shown in Fig. 2.15, the curves exhibits error floors below a certain value of the BER. In the next chapter, further investigation of the technique is provided using EXIT chart analysis for which the analysis of the BER floor property shown in Fig. 2.15.

Chapter 3

EXIT Chart Analysis

This chapter is started with the fundamental principle of EXIT Chart. Furthermore, EXIT analysis of the SPCCIRC-BICM-ID EM previously introduced in Chapter 2 is provided.

3.1 Fundamental Principle: Entropy and Mutual Information

Entropy is a measure of the uncertainty of a random variable. The entropy $H(B)$ of source information b emitted from the source B is defined by

$$H(B) = -\sum_{b \in B} P_r(b) \log P_r(b). \tag{3.1}$$

Conditional Entropy $H(B|L)$, which indicates the entropy of information source B given LLR L, as

$$\begin{aligned} H(B|L) &= \sum_{l \in L} P_r(b) H(B|L=l) && (3.2)\\ &= -\sum_{b \in B} P_r(b) \sum_{l \in L} P_r(l|b) \log P_r(l|b) && (3.3)\\ &= -\sum_{b \in B} \sum_{l \in L} P_r(b,l) \log P_r(l|b) && (3.4)\\ &= -E[\log P_r(b|l)] && (3.5) \end{aligned}$$

MI between B and L, $I(B;L)$ can be expressed as

$$\begin{aligned} I(B;L) &= H(B) - H(B|L) && (3.6)\\ &= H(L) - H(L|B) && (3.7) \end{aligned}$$

Therefore, MI between B and L can be understood as the reduction of uncertainty of $B(L)$ by knowing $L(B)$, Since the appearance probability of the binary information source 0 and 1 is equiprobable, from (2.1).

$$H(B) = 1 \tag{3.8}$$

Therefore, under the assumption, MI can be expressed as following,

$$I(B;L) = 1 - H(B|L). \tag{3.9}$$

From [4], MI between B and L can expressed as following,

$$\begin{aligned} I(B;L) &= \sum_{b\in B}\int_{l\in L} P_r(b,l)\log_2\frac{P_r(b,l)}{P_r(b)P_r(l)}dl && (3.10)\\ &= \sum_{b=+1,-1}\int_{-\infty}^{+\infty} P_r(l|b)P_r(b)\log_2\frac{P_r(l|b)}{P_r(l)}dl && (3.11)\\ & && (3.12) \end{aligned}$$

Now assume that $b = 0$ and $b = 1$ are equiprobable, i.e,

$$P_r(b=+1) = P_r(b=-1) = \frac{1}{2}. \tag{3.13}$$

Then, the following holds;

$$\begin{aligned} P_r(l) &= P_r(b=+1)P_r(l|b=+1) + P_r(b=-1)P_r(l|b=-1)\\ &= \frac{1}{2}\{(l|b=+1) + P_r(l|b=-1)\}. \end{aligned} \tag{3.14}$$

Furthermore, using (3.14),

$$I(B;L) = \frac{1}{2}\sum_{b=+1,-1}\int_{-\infty}^{\infty} P_r(l|b)\log_2\frac{2P_r(l|b)}{P_r(l|b=+1)+P_r(l|b=1)}dl. \tag{3.15}$$

Because of the symmetricity property of probability distribution function

$$P_r(l|b=+1) = P_r(-l|b=-1) = \frac{1}{\sqrt{2\pi}\sigma}e^{-\frac{(l\mp1)^2}{2\sigma^2}} \tag{3.16}$$

following holds;

$$I(B;L) = \int_{-\infty}^{+\infty} P_r(l|b=+1)\log_2\frac{2P_r(l|b=+1)}{P_r(l|b=+1)+P_r(-l|b=+1)}dl. \tag{3.17}$$

Also by the consistency condition $P_r(-l|b=+1) = e^{-l}P_r(l|b=-1)$,

$$I(B;L) = \int_{-\infty}^{+\infty} P_r(l|b=+1) log_2 \frac{2}{1+e^l} dl = 1 - E[\log_2(1+e^{-l})] \tag{3.18}$$

holds. [4] shows that by invoking the Ergodicity of LLR, (3.18) can be approximated by;

$$I(B;L) = 1 - E[\log_2(1+e^{-l})] \approx 1 - \frac{1}{K}\sum_{k=1}^{K} \log_2(1+e^{-l_k \cdot b_k}). \tag{3.19}$$

3.2 J-Function

It is found from (3.16) that if the LLR follows Gaussian distribution, MI is a function of the variance of the LLR. Therefore, the variance of LLR and MI is connected by

$$J(\sigma) = I(\sigma_L = \sigma), \tag{3.20}$$

where $J(\cdot)$ is referred to as J-function. If it is required to evaluated exactly the J-function, a numerical integration technique for (3.17) has to be used by measuring the probabilities $P_r(l|b=+1)$ and $P_r(l|b=-1)$. However, the following approximation has been widely used because of its high accuracy.

$$J(\sigma) = (1 - 2^{-H_1\sigma^{2H_2}})^{H_3} \tag{3.21}$$

and

$$J^{-1}(I) = (-\frac{1}{H_1}\log_2(1 - I^{\frac{1}{H_3}})))^{\frac{1}{2H_2}} \tag{3.22}$$

with $H_1 = 0.3073, H_2 = 0.8935$ and $H_3 = 1.1.064$ for 4-QAM.

3.3 EXIT Chart

EXIT chart is used to analyse and design iterative systems such as SPCCIRC-BICM-ID-EM. MI input/output of the demapper and decoder is drawn on EXIT chart. Artificial LLR sequence having MI input for I can be created by using the inverse J-function, as

$$l_k = \frac{(J^{-1}(I))^2}{2} b_k + \nu_k J^{-1}(I), \tag{3.23}$$

where the equivalent noise ν_n follows a zero mean Gaussian distribution with variance σ^2. Using the artificial LLR generated from demapper *a priori* MI $I_{dem,a}$ and received signal y, demapping is performed as in (2.14) and *extrinsic* LLR output is used in (3.19) to obtain output MI $I_{dem,e}$. Demapping process for drawing the demapper EXIT curve is depicted on Fig. 3.1. In the same way, decoder uses the artificial LLR

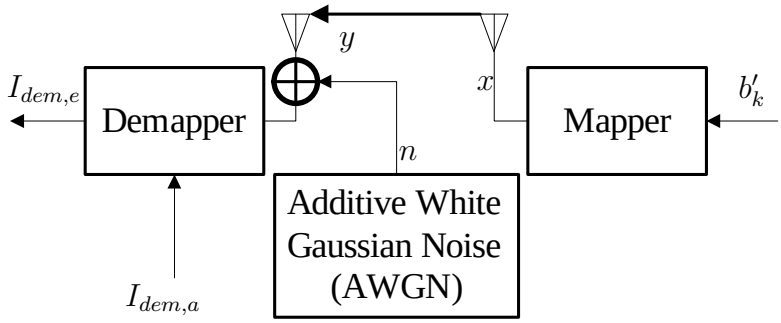

Figure 3.1: Variables used for Demapper EXIT Curve

corresponding to the *a priori* MI input $I_{dec,a}$ to perform decoding and output MI $I_{dec,e}$ is obtained from the LLR output of the decoder. For the decoder, this process can be approximated using mathematical equation witch will be explained in detail in section 3.6. Fig. 3.2 shows the typical EXIT Chart. For the demapper EXIT curves X-and Y-axis corresponds to the a priori and extrinsic MI, respectively, while for the decoder EXIT curve, vise-versa. Moreover, in Fig. 3.2, a trajectory representing the actual MI exchange, iteration-by-iteration, obtained by the chain simulation. If, in general, convergence property of a turbo system follows, as it is designed, the trajectory and EXIT curves should exactly matches.

3.4 Properties of EXIT Chart

Following characteristics of iterative communication systems can be analysed by the EXIT analysis:

- **Constellation Constrained Capacity (CCC)**: The area A_{dem} under the demmaper EXIT curve corresponds to the CCC, the capacity of the system using non-Gaussian constellation points for modulation.
- **Code Rate**: The area A_{dec} under the decoder EXIT curve corresponds to the code rate R.
- **Distance to the Shannon limit**: The gap between the two EXIT curves corresponds to the rate loss or, in other words, distance to the Shannon limit in bit rate.
- **Required Number of Iterations**: Trajectory is used to observe how the extrinsic information has been exchanged in the real chain between the demapper and the channel decoder. A pair of one horizontal and one vertical increases in MI refers to one turbo loop iteration. When the area between the two EXIT curves is increased due to the rate loss, each steps of trajectory becomes larger.

Consequently making the required iteration number low. Therefore, distance to the Shannon limit (loss in bit rate.) and number of required iterations are in the relation of trade-off.

- **Expected BER**: If the two EXIT curves intersects, no more gain in MI can be achieved by the iterations. By evaluating the decoder's *a posteriori* MI $I_{dec,a}$ at the intersection point, BER can be estimated by

$$BER = \frac{1}{2}\text{erfc}\left(\frac{J^{-1}(I_{dec,p})}{2\sqrt{2}}\right), \tag{3.24}$$

  where $I_{dec,p}$ is *a posteriori* MI between the transmitted information bit and *a posteriori* LLR. The area between the two EXIT curves is called convergence tunnel. If the convergence point is open until $(1.0, 1.0)$ MI point without intersection, BER can be arbitrary eliminated because $J^{-1}(I_{dec,p} = 1) \to \infty$

In theory, if, with a BICM-ID system, $A_{dem} > A_{dec}$ so that the convergence tunnel is open until $(1.0, 1.0)$ MI point, arbitrarily small BER can be achieved If $A_{dem} = A_{dec}$, such BICM-ID system can achieve the Shannon limit. However, if $A_{dem} = A_{dec}$ MI exchange can not be initiated, and hence in practice, $A_{dem} \gtrapprox A_{dec}$.

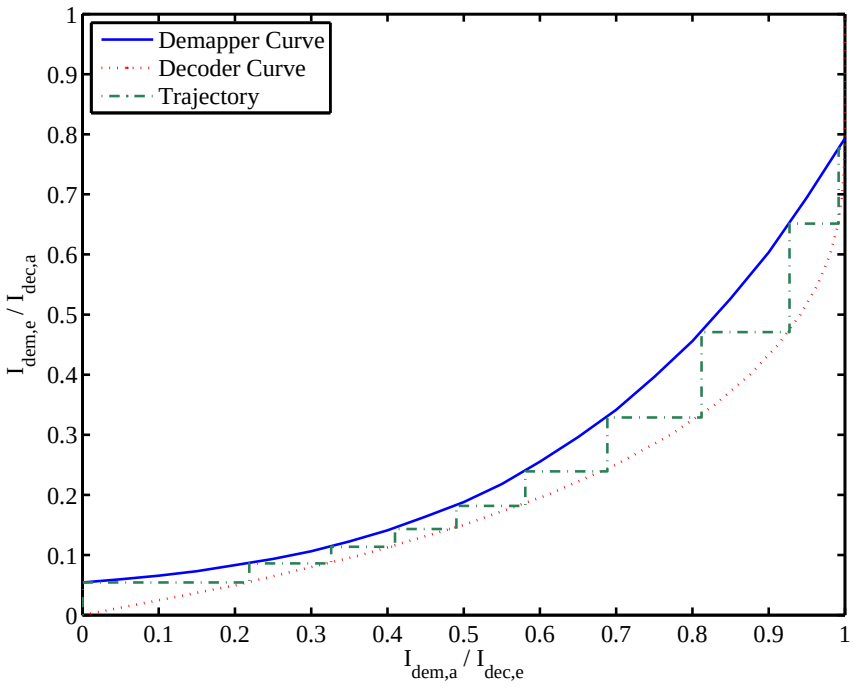

Figure 3.2: General EXIT chart

3.5 Demapper EXIT Curve

In SPCCIRC-BICM-ID, the shape of demapper EXIT curve depends on the SNR and the labelling pattern. EM with different labelling pattern have the same area under the demapper EXIT curve having different shape. This is because the CCC is not dependent on the labelling pattern[1].

3.6 Decoder EXIT Curve

Decoder EXIT curve can be expressed mathematically. For deeper understanding, this thesis start from the simple example, repetition code. The repetition code can be obtained by simply repeating the information bit d_v times. With the Gaussian assumption for the LLR distribution, the EXIT function of the repetition code is given analytically by,

$$I_{dec,e} = J(\sqrt{(d_v - 1) \cdot J^{-1}(I_{dec,a})^2}), \tag{3.25}$$

where $I_{dec,a}$ is a priori MI and $I_{dec,e}$ is the extrinsic MI. $J(\cdot)$ and $J^{-1}(\cdot)$ are the functions that convert the square-root variance σ_n of LLR to its corresponding MI, and its inverse, respectively. Obviously, (3.25) is corresponding to the second term in (2.17) for updating LLR, with which $I_{dec,a} = I_{dem,e}$ with $I_{dem,e}$ being the demapper's output extrinsic MI.

With the Gaussian assumption for the LLR distribution, the check node EXIT function can be approximated with high enough accuracy by,

$$I_{cnd,e} = 1 - J(\sqrt{d_c - 1} \cdot J^{-1}(1 - I_{cnd,a})) \tag{3.26}$$

where

$$I_{cnd,a} = J(\sqrt{d_v \cdot J^{-1}(I_{dec,a})^2}) \tag{3.27}$$

The EXIT function of the whole decoder comprised of the variable and check node decoders can be calculated by combining (3.28) and (3.27), as

$$I_{dec,e} = J(\sqrt{(d_v - 1) \cdot J^{-1}(I_{dec,a}^2 + J^{-1}(I_{cnd,e})^2)}) \tag{3.28}$$

with $I_{dec,a} = I_{dem,e}$ For the check node assisted irregular repetition code, the EXIT function of the whole decoder can be obtained by weighting the segment-wise EXIT functions given by (3.28), according to their distributions a_i, as

$$I_{dec,e} = \frac{\sum_i a_i \cdot d_{v,i} \cdot J(\sqrt{(d_{v,i} - 1) \cdot J^{-1}(I_{dec,a}^2) + J^{-1}(I_{cnd,e})^2})}{\sum_i a_i \cdot d_{v,i}} \tag{3.29}$$

[1]Precisely speaking, this is not true, but the difference is very small. The CCC is different, depending on the labelling pattern, only in the area where CCC curve deviates for the Gaussian capacity

Hence, the shape of the EXIT curve of the code can be flexibly controlled by the irregular degree allocations.

3.7 EXIT Chart Analysis

Fig. 3.3, Fig. 3.4 and Fig. 3.5 are the EXIT Chart of SPCCIRC-BICM-ID-EM for SNR = 0.6, 0.9 and 2.0 in decibels, respectively. Degree allocations are $d_c = 80$, $\{d_{v1}, d_{v2}\} = \{5, 7\}$ and $\{a_1, a_2\} = \{0.77, 0.23\}$. Note that this degree allocations are obtained empirically. In Fig. 3.3, it can be observed that demapper and decoder EXIT curve intersect around the $(0.3, 0.1)$ MI point. Consequently, trajectory can not go through the intersection point.

As mentioned in section 3.4, when the two EXIT curves crosses and trajectory stops at a point apart from $(1.0, 1.0)$ MI point, higher BER is expected. In actual BER simulation, it can be observed from corresponding BER curve in Fig. 2.15, relatively high BER performance presented with SNR = 0.6 dB. In Fig. 3.4, where SNR = 0.9 dB, demapper EXIT curve is lifted up compared to the curve in Fig. 3.3.

On the other hand, decoder EXIT curve stays the same. Increase in area below the demapper curve observed by comparing Fig. 3.3 and 3.4 indicates the increase in the channel capacity due to increased SNR. In Fig. 3.4, the narrow tunnel between the demapper and decoder EXIT curve is found to be open until a point (X, Y) where X is very close to 1.0. This narrow tunnel allows the trajectory to sneak through and reach around $(1.0, 0.7)$ MI point.

Reducing the SNR to 0.6 dB push down the demapper EXIT curve, and thereby, change the intersection point of the two curves from $(1.0, 0.7)$ with SNR = 0.9 dB to the point around $(0.3, 0.1)$. Consequently, turbo cliff happens at a certain SNR, around which tow curves intersect, and the MI corresponding to the intersection point suddenly decreases to a very low value; the intersection point can be found by slightly increasing/decreasing the SNR value and observing their corresponding EXIT curves.

In fact, turbo cliff can be observed at around SNR = 0.9 dB in Fig. 2.15. In Fig. 3.5, demapper curve is further lifted up by increasing the SNR to 2.0 dB. As mentioned in section 3.4, gap between the two curves corresponds to the loss in bit rate and hence smaller spectrum efficiency when the system is operated at SNR = 2.0 dB. Corresponding by, it can be observed from the BER curve in Fig. 2.15 that distance from the 2.0 dB SNR to the the Shannon limit quite far and hence less spectrum efficient with this operation point. However, it is observed from Fig. 3.5 that number of the iterations (pair of vertical and horizontal iterations in MI) is smaller than that of Fig. 3.4 and Fig. 3.3 due to the larger gap between the two EXIT curves. Therefore, it can be stated that in higher SNR range, spectrum efficiency loss is incurred while number of iteration is reduced.

For the SPCCIRC-BICM-ID-EM with degree allocation $d_c = 100, \{d_{v1}, d_{v2}, d_{v3}\} = \{3, 5, 6\}$ and $\{a_1, a_2, a_3\} = \{0.51, 0.41, 0.01\}$ the same tendency is observed where

SNR is varied. The EXIT chart for the SPCCIRC-BICM-ID-EM with the parameters shown above is depicted on Fig. 3.6. In the next chapter, it is shown that the optimal degree allocation can systematically determined using LP.

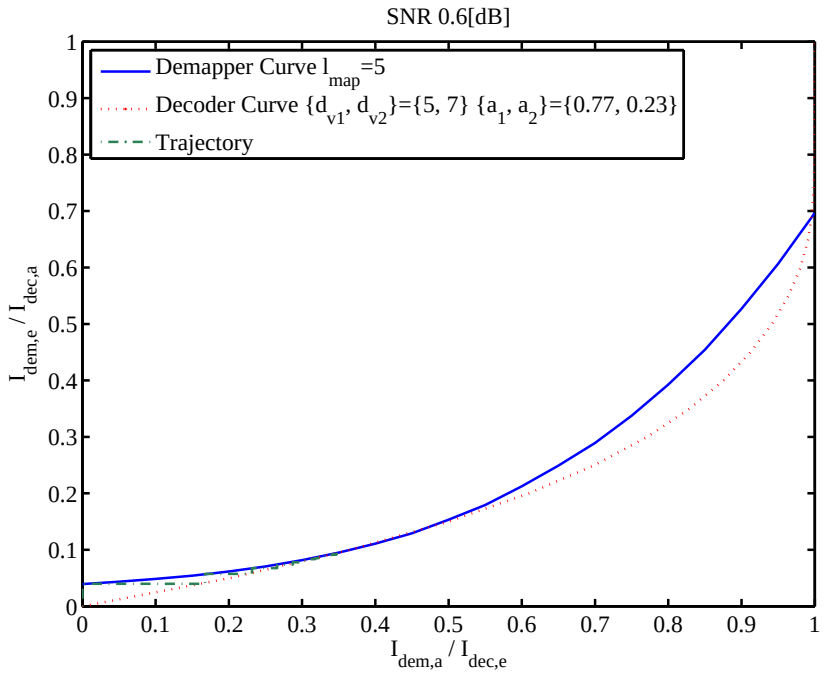

Figure 3.3: EXIT Chart of SPCCIRC-BICM-ID-EM at SNR = 0.6 dB

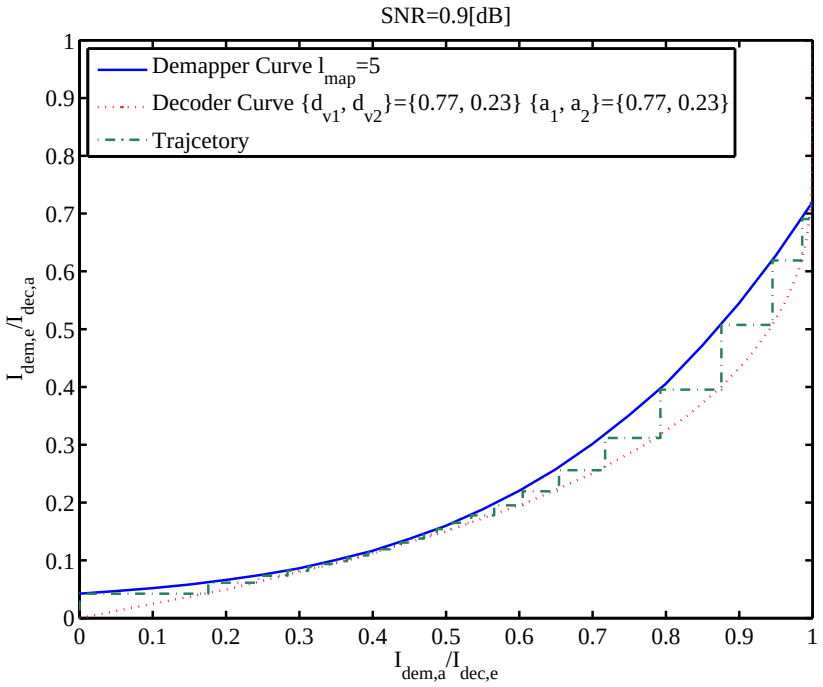

Figure 3.4: EXIT Chart of SPCCIRC-BICM-ID-EM at SNR = 0.9 dB

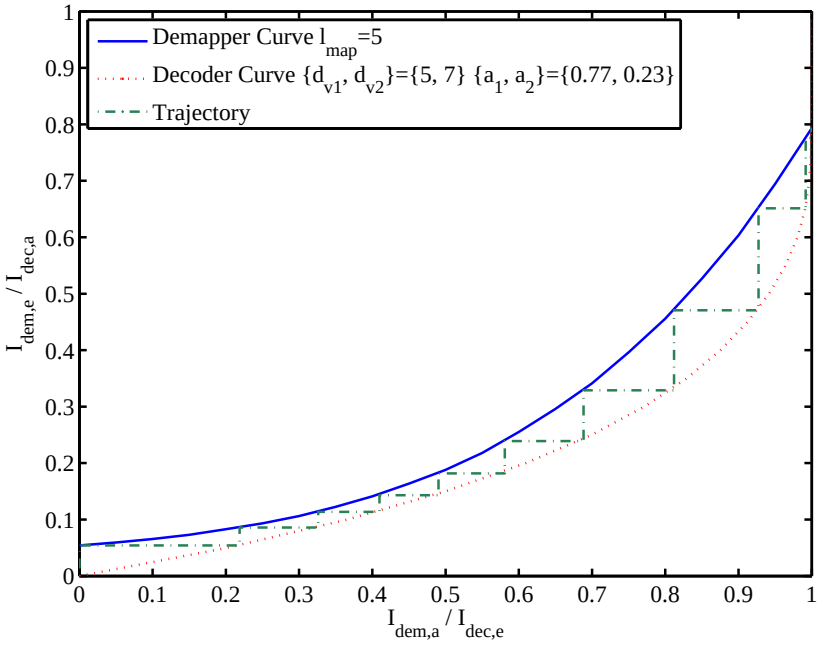

Figure 3.5: EXIT Chart of SPCCIRC-BICM-ID-EM at SNR = 2.0 dB

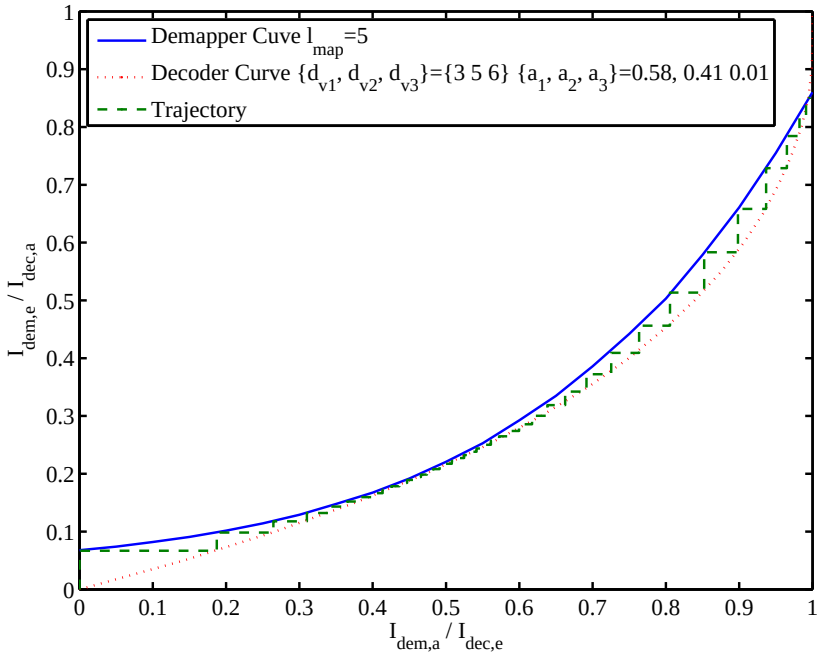

Figure 3.6: EXIT Chart of SPCCIRC-BICM-ID-EM at SNR = 3.1 dB

Chapter 4

Optimization of Node Degree Allocation using LP

As explained in Chapter. 3, since SPCCIRC-BICM-ID-EM is a serially concatenated system, its power efficiency and convergence property can be evaluated using the EXIT chart. It has also been mentioned that when the demapper and decoder EXIT curves are closely enough matched, while the convergence tunnel opens until a point near enough to the $(1.0, 1.0)$ MI point, clear threshold in BER performance curve can be achieved, and the distance in achievable bitrate from the channel capacity corresponds to the area between the two EXIT curves. In the work that first introduced SPCCIRC-BICM-ID-EM [5][11], however, the degree allocation were obtained empirically, and no systematic technique was presented. In this chapter, it is shown that determining the optimal irregular degree allocation falls into a convex optimization problem, for which it can be solved via LP techniques.

4.1 Criterion

The goal of finding the optimal irregular degree allocation is to approach, and ultimately to achieve the Shannon limit. Therefore, maximizing the code rate is the primal goal in designing the SPCCIRC-BICM-ID-EM system having the optimal irregular degree allocation, given the channel's SNR. However, simply maximizing the code rate may degrade the BER performance of the system because the relationship between capacity and SNR is one-to-one mapping, and code design have to be performed very carefully. As mentioned in Section 2.4, to achieve arbitrary low BER, the code rate must not exceed the channel capacity. From the viewpoint of the EXIT characteristics, code rate exceeding the channel capacity corresponds to the case where the area A_{dec} below the decoder EXIT curve is larger than the area A_{dem} below the demapper EXIT curve. This will consequently makes the trajectory to stack at a point far from the $(1.0, 1.0)$ MI point on the EXIT chart, and the perfor-

mance degrades. Moreover, even the code rate is smaller than the channel capacity, there is a possibility that the demapper EXIT curve and the decoder EXIT curve intersect. Therefore, designing BICM-ID system such that the intersection point is as close to the $(1.0, 1.0)$ MI point as possible is of significant important factor when achieving steeper drop in BER at turbo cliff is aimed at. Moreover, it has to be always considered that summation of node degree allocations have to be always 1. Now the criteria for the optimal design can be summarized as follows:

1. Code rate has to be lower than but as close to the capacity as possible.
2. Keep the convergence tunnel open between the demapper and decoder EXIT curve until the desired crossing point and the point should be as close to the $(1.0, 1.0)$ MI point as possible.
3. Summation of node degree allocations has to be always 1.

4.2 Linear Programming

The previously introduced criteria can be, given l_{map}, written as

$$\begin{aligned} &\text{Find } a_i \text{ for each } d_{v,i} \\ &\text{Such that Rate} = (d_c - 1)/(d_c \sum_i a_i \cdot d_{v,i}) \rightarrow \text{Maximized} \\ &\text{Subject to } \sum_i a_i = 1, \\ &\qquad \text{and } I_{dec,e} > I_{dec,a} = I_{dem,e}, \end{aligned} \tag{4.1}$$

where $I_{dec,e}, I_{dec,a}$ and $I_{dem,e}$ denote the decoder *extrinsic* MI, the decoder *a priori* MI and the demapper *extrinsic* MI, respectively. Now, assume that the check node degree d_c is a fixed constant. Then, the optimality criteria of (4.1) is equivalent to

$$\begin{aligned} &\text{Find } a_i \text{ for each } d_{v,i} \\ &\text{Such that } \sum_i a_i \cdot d_{v,i} \rightarrow \text{Minimized} \\ &\text{Subject to } \sum_i a_i = 1 \\ &\qquad \text{and } I_{dec,e} > I_{dec,a} = I_{dem,e} \end{aligned} \tag{4.2}$$

Here, index w is introduced, which is representing the MI point, and also another parameter ϵ_w representing the acceptable gap between $I_{dec,e}$ and $I_{dec,a}$, such that

$$\begin{aligned} I_{dec,e,w} - I_{dec,a,w} \geq \epsilon_w \geq 0 \\ \text{for } 1 \leq w \leq N, \end{aligned} \tag{4.3}$$

where N is the number of the constraint points on the EXIT curve, indexed by w. (4.3) can be expressed as.

$$\begin{aligned}
&I_{dec,e,w} - I_{dec,a,w} \geq \epsilon_w > 0 \\
&\Leftrightarrow \frac{\sum_i a_i \cdot d_{v,i} \cdot J(\sqrt{(d_{v,i}-1)\cdot J^{-1}(I_{dem,e,w})^2 + J^{-1}(I_{cnd,e,w})})}{\sum_i a_j \cdot d_{v,i}} - I_{dem,a,w} > \epsilon_w \\
&\Leftrightarrow \sum_i a_i \cdot d_{v,i} \cdot J(\sqrt{(d_{v,i}-1)\cdot J^{-1}(I_{dem,e,w})^2 + J^{-1}(I_{cnd,e,w})}) \\
&- I_{dem,a,w} \cdot \sum_i a_i \cdot d_{v,i} > \epsilon_w \cdot \sum_i a_i \cdot d_{v,i} \\
&\Leftrightarrow \sum_i a_i \cdot d_{v,i} \cdot (-J(\sqrt{(d_{v,i}-1)\cdot J^{-1}(I_{dem,e,w})^2 + J^{-1}(I_{cnd,e,w})} \\
&+ I_{dem,a,i} + \epsilon_w)) < 0
\end{aligned} \tag{4.4}$$

Therefore, (4.3) can be regarded as the linear function of a_i. Now the optimality criterion can be rewritten with the parameters and indexes defined above, as

$$\begin{aligned}
&\text{Minimize } \sum_i a_i d_{v,i} \\
&\text{Subject to} \\
&\sum_i a_i \cdot d_{v,i} \cdot (-J(\sqrt{(d_{v,i}-1)\cdot J^{-1}(I_{dem,e,w})^2 + J^{-1}(I_{cnd,e,w})}, \\
&+ I_{dem,a,w} + \epsilon_w)) < 0 \ \ (\text{for } 1 \leq w \leq N) \\
&\text{and } \sum_i a_i = 1
\end{aligned} \tag{4.5}$$

An illustrative diagram of this concept is shown in Fig. 4.1 where $1 \leq w \leq 11$. Now, given the fact that the optimization parameter in (4.5) is only a_i and the other terms are fixed constant. Furthermore, the index function and constraints are both convex in terms of the optimization variable a_i. Therefore, the problem falls into very simple convex optimization, solvable by using LP techniques. For finding the optimal check node degree d_c, this thesis proposes a brute-force search (or all possible value search), as summarized in **Algorithm 1**.

4.3 EXIT Chart Analysis

Table 4.1 and 4.2 show, as an example, the degree allocation optimization for $l_{map} = 5, d_c = 21$ and SNR = 0.9 dB, where the simplex algorithm was used as a tool for linear programming tool. Table4.3 show the initial values of ϵ for the optimization and Table 4.2 shows the results. Fig. 4.2 shows the entire portion of the EXIT

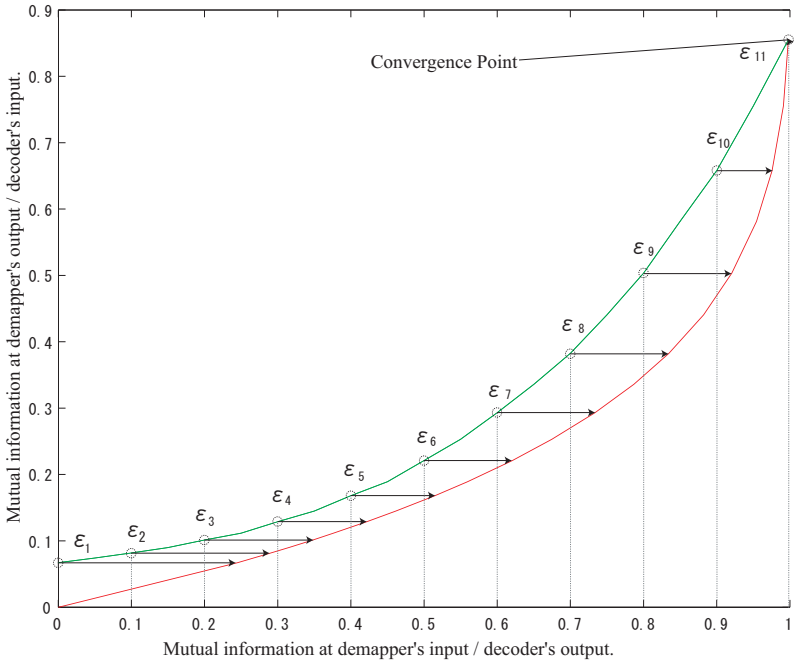

Figure 4.1: Example of ϵ Settings

curves for the demapper, decoder with and without optimal degree allocations. In the case without degree optimization, the empirically obtained distribution shown in [5], [11] is used. The two decoder curves are very close each other, but this is due mainly to the coincidence. Fig. 4.3 and Fig. 4.4 also shows the middle and ending parts of the EXIT chart, in the range of $0.385 \leq I_{dem,input} \leq 0.42$, and $0.98 \leq I_{dem,input} \leq 1.0$, respectively. It is found that the proposed optimization technique using linear programming achieves smaller gap between the demapper and decoder curves. With the same initial degree settings, Fig. 4.5 shows the EXIT curves with and without optimization for SNR = 3.1 dB. Intersection point of the two curves

Algorithm 1 Brute force search and LP algorithm

Initialize d_{vi} and a_i values.
for $d_c = 1$ **to** $\max d_c$ **do**
  Perform LP for d_c and obtain optimal distribution a_i for each d_{vi}.
  Calculate code rate $R_{SPCCIRC}$ using d_c and a_i.
end for
Find $d_{c,opt}$ and a_{opt} achieving $R_{SPCCIRC} \rightarrow \max$.
return $d_{c,opt}$ and a_{opt}.

are now relatively closer to the empirically designed case. However, with SNR 3.1 dB, the code rate from LP is a little smaller than the code rate obtained from empirically obtained degree allocation. Therefore, lower BER with lower spectrum efficiency is expected in this case.

Table 4.1: Degree Distributions Before Optimization

d_v	1	2	3	4	5	6	7	8	9	10
a	$\frac{1}{10}$	$\frac{1}{10}$	$\frac{1}{10}$	$\frac{1}{10}$	$\frac{1}{10}$	$\frac{1}{10}$	$\frac{1}{10}$	$\frac{1}{10}$	$\frac{1}{10}$	$\frac{1}{10}$

Table 4.2: Degree Distributions Obtained by the Optimization

d_v	1	2	3	4	5	6	7	8	9	10
a	0	0	0	0	0.993	0.004	0	0	0	0.003

Table 4.3: ϵ Settings

w	1	$\cdots$	5	6	7	8	9	10	11	$\cdots$	20
ϵ_w	0	$\cdots$	0	0.001	0.001	0.001	0.001	0.001	0	$\cdots$	0

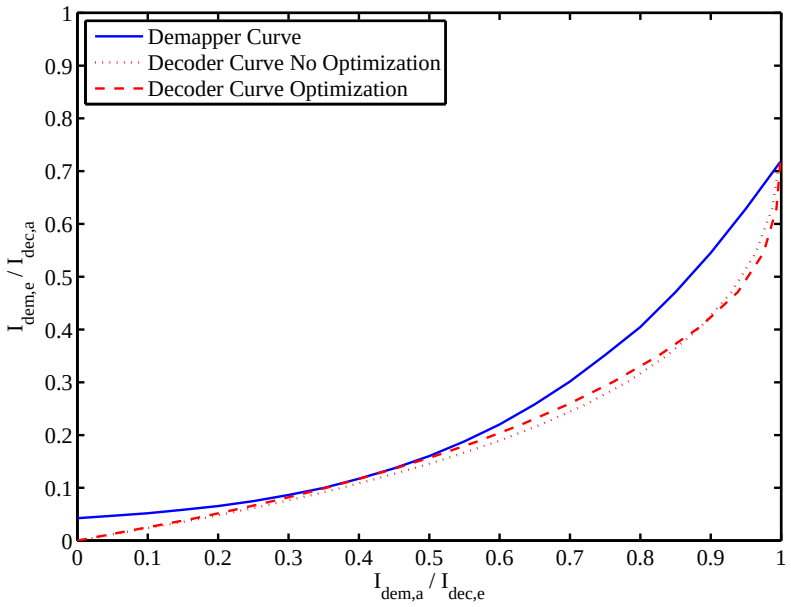

Figure 4.2: EXIT Curves of Demapper and Decoder with/without Degree Optimization at SNR = 1.0 dB

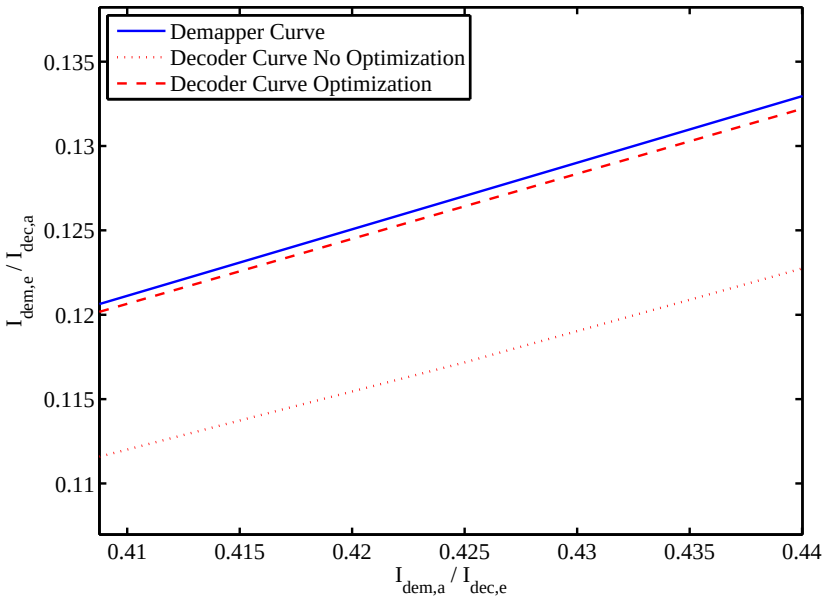

Figure 4.3: The Detail of EXIT Curves of Demapper and Decoder with/without Degree Optimization around MI = 0.4 at SNR = 1.0 dB

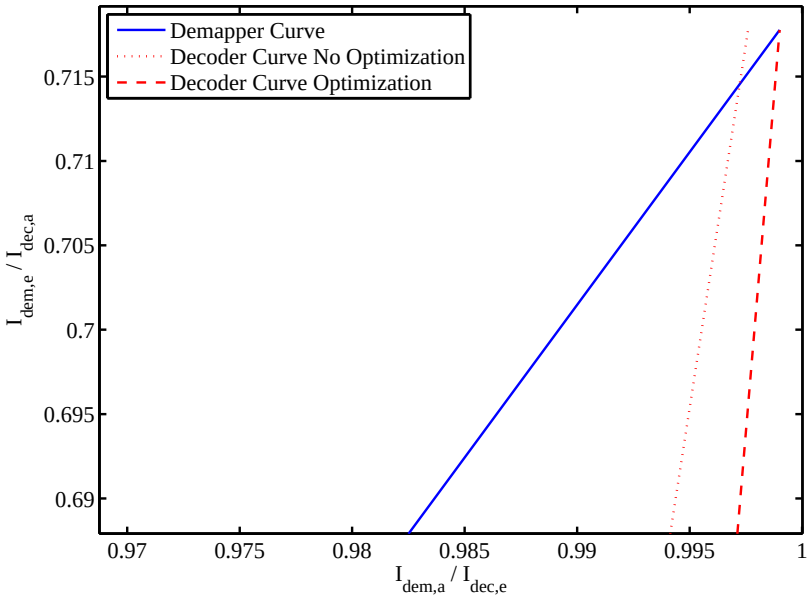

Figure 4.4: The Detail of EXIT Curves of Demapper and Decoder with/without Degree Optimization around MI = 1.0 at SNR = 1.0 dB

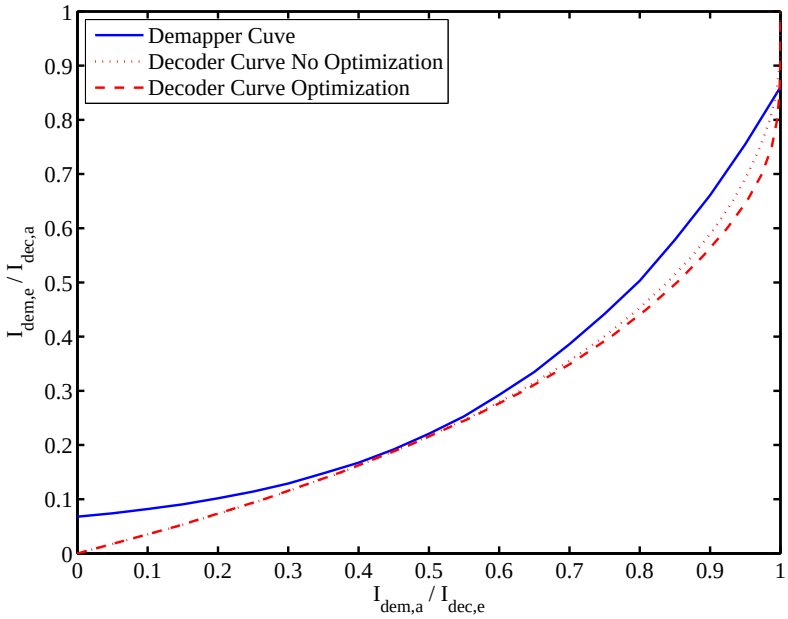

Figure 4.5: EXIT Curves of Demapper and Decoder with/without Degree Optimization at SNR = 3.0 dB

Chapter 5

Partial Accumulator Aided SPCCIRC-BICM-ID-EM

In the previous chapter, degree allocation using LP was presented, where it was shown that SPCCIRC-BICM-ID-EM with optimal degree allocation obtained by LP can achieve higher spectrum efficiency. However, even with the use of LP technique, arbitrary low BER can not be achieved. This is because the right most point of the demapper EXIT curve does not reach $(1.0, 1.0)$ MI point and hence the demapper and the decoder EXIT curve cross at a point (X, Y) where point X is very close to 1.0 but Y is still far apart from 1.0. In this chapter, rate-1 partial accumulator is introduced to lift up the right most point of the demapper EXIT curve to reach $(1.0, 1.0)$ MI point.

5.1 Partial Accumulator

[12] suggests that by using the memory-1 rate-1 recursive systematic convolutional codes , referred to as accumulator that follows interleaver located after the encoder, the BER floor of BICM-ID system can be eliminated. Furthermore, it was shown by [13] that by transmitting one accumulator output bit $\hat{b}_k$ only to replace the channel encoded bit b'_k at every P bits, referred to as doping ratio (1:P), fine matching of the EXIT curves is possible. This thesis introduces the use of rate-1 partial accumulator aided SPCCIRC-BICM-ID-EM as depicted on Fig. 5.1. The system, partial accumulator aided SPCCIRC-BICM-ID-EMis referred to as PA-SPCCIRC-BICM-ID-EM later on, and its functional diagram representing the process of partial accumulator is shown in Fig. 5.2. The process for partial accumulator be simply described by

$$\bar{b}_k = \bar{b}_{k-1} \oplus b'_k \tag{5.1}$$

$$\hat{b}_k = \begin{cases} b'_k & \text{for } k \mod P \neq 0 \\ \bar{b}_k & \text{for } k \mod P = 1 \end{cases} \tag{5.2}$$

where, with the k denoting the bit timing index after interleaving k mod P indicates modulo-P operation for k.

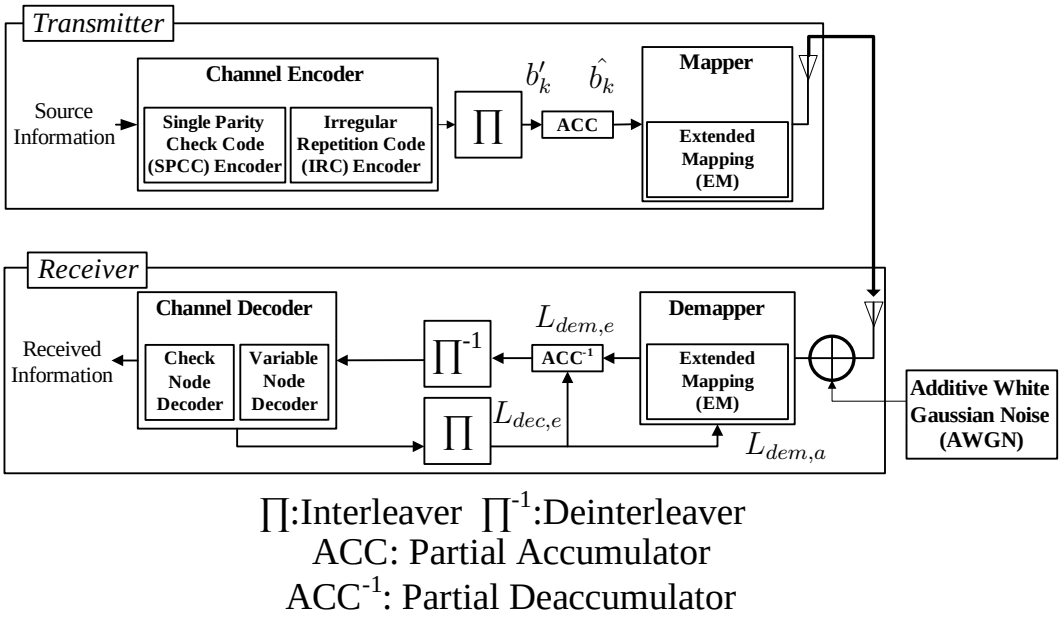

Figure 5.1: Partial Accumulator Applied SPCCIRC-BICM-ID-EM

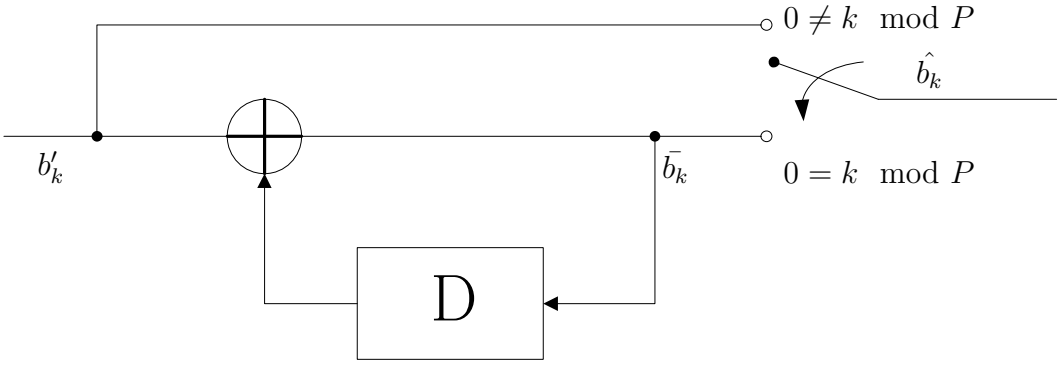

Figure 5.2: Partial Accumulator

5.2 Decoding of Partial Accumulator

For de-accumulation at the receiver side, Bahl-Cocke-Jelinek-Raviv (BCJR) decoding is performed. To describe the process of BCJR, trellis diagram is used. The trellis diagram describes which transitions at a certain time are possible and what input bit is necessary to cause this transition. The trellis diagrams consist of nodes and edges. Each node represents one state of the delay taps in the encoder, and the edges show

which transitions are possible from the node. At the receiver, the a priori information on the coded bits is thus provided to the BCJR decoder for the rate-1 code, while the a priori information on the information bits is fed into the demapper. Due to the code doping, the input branches to the de-accumulator have to be properly controlled. The branch metric in the BCJR algorithm is defined as

$$\gamma(s, s') = exp\left(\frac{b' L_{dec,e} + \hat{b} L_{dem,e}}{2}\right) \tag{5.3}$$

with the *a priori* infomation of ACC^{-1} being

$$L_{dec,e} = \begin{cases} 0, & k \mod P \neq 0 \\ L_{dec,e}, & k \mod P = 0 \end{cases} . \tag{5.4}$$

On the other hand, the *a priori LLR* of the demapper,

$$L_{dem,a} = \begin{cases} L_{dec,e}, & k \mod P \neq 0 \\ 0, & k \mod P = 0 \end{cases} \tag{5.5}$$

Fig. 5.3 shows the trellis diagram for the BCJR algorithm.

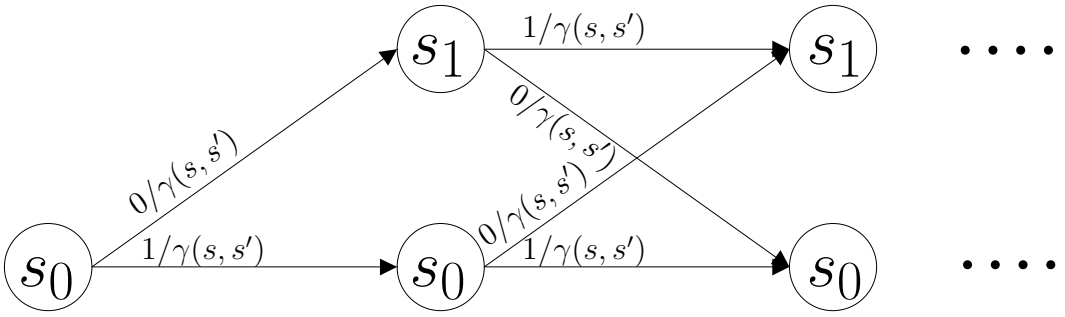

Figure 5.3: Trellis Diagram

5.3 EXIT Chart Analysis

Fig. 5.4 shows the EXIT curve for demapper+ACC^{-1} for $P = \{50, 100, 150, 200\}$. It can be observed that all demapper curves can achieve right-most point close enough to the $(1.0, 1.0)$ MI point. Furthermore, P values affect the shape of the demapper curve. In Fig. 5.5, it can be observed that the larger the P value, the sharper the decay of the curve around $(1.0, 1.0)$ MI point. Fig. 5.6 shows the EXIT curve for demapper + ACC^{-1} with $P = 200$ for SNR = 1.0 dB. In addition, two decoder EXIT

curves are drawn. One is using the empirically obtained degree allocation [5] and the other is using the degree allocation obtained from using LP. It can be observed from Fig. 5.6 that the demapper and decoder EXIT curves closely match except the left-most region. Similar result can be observed from Fig. 5.7 where SNR is 3.1 dB. Both in Fig. 5.6 and Fig. 5.7, two EXIT curves crosses at a point close to $(1.0, 1.0)$ MI point. Therefore, no BER floor is expected after the turbo cliff.

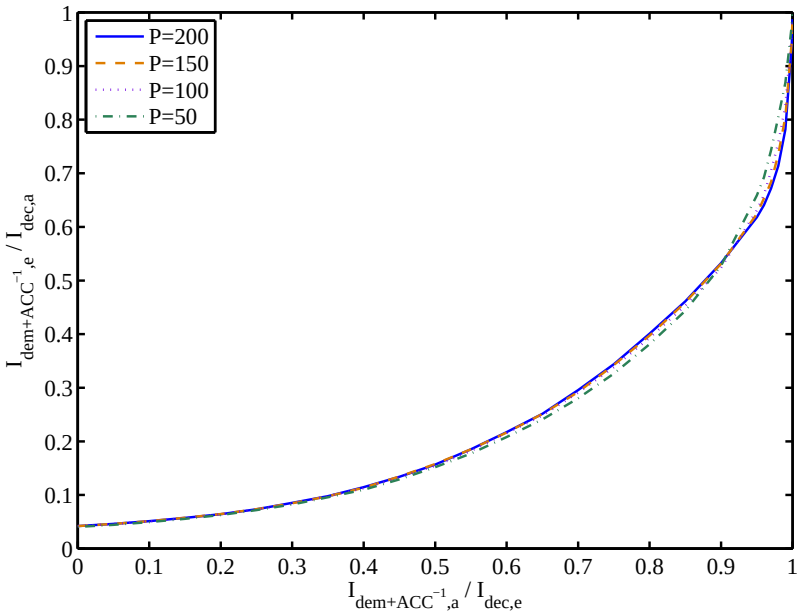

Figure 5.4: Demapper Curves with Several P Values at SNR = 1.0 dB

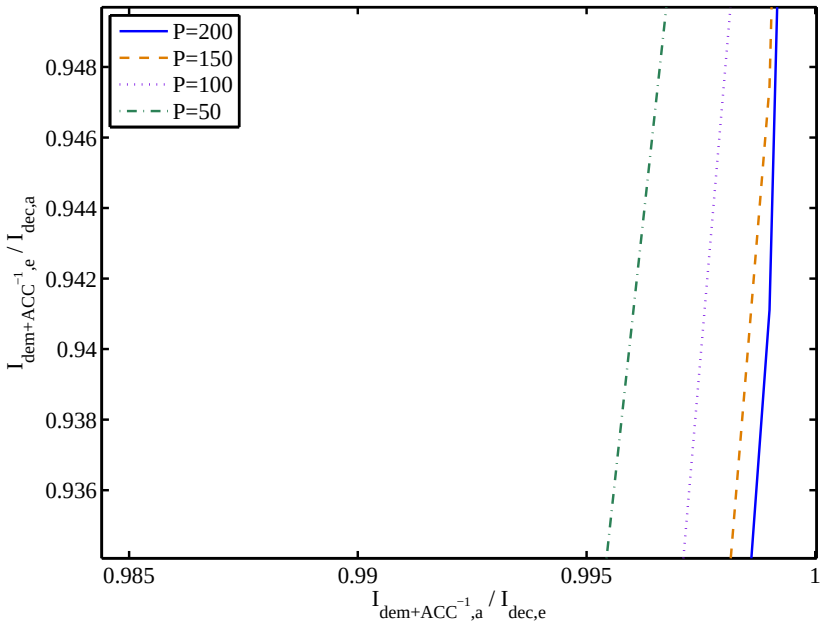

Figure 5.5: Demapper Curves with Several P Values around MI = 1.0 at SNR = 1.0 dB

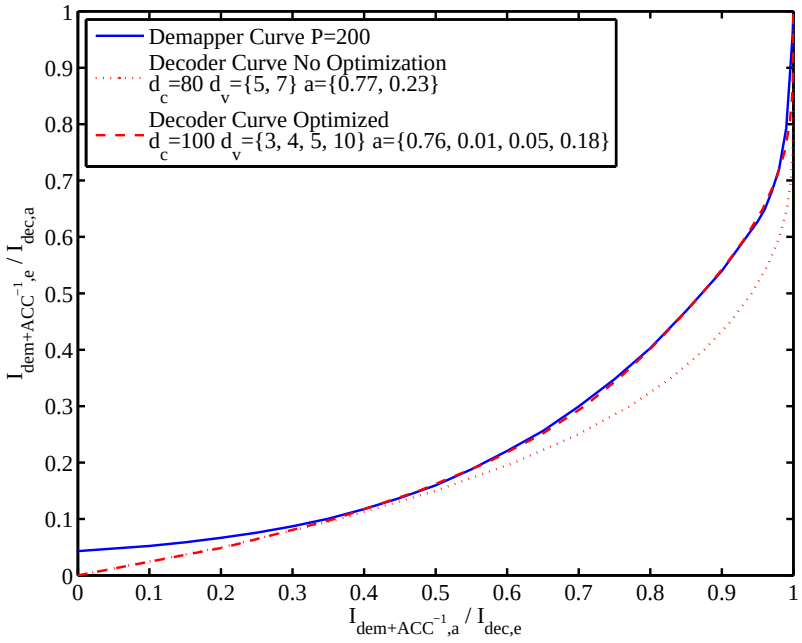

Figure 5.6: EXIT Chart using Partial Accumulator at SNR = 1.0 dB

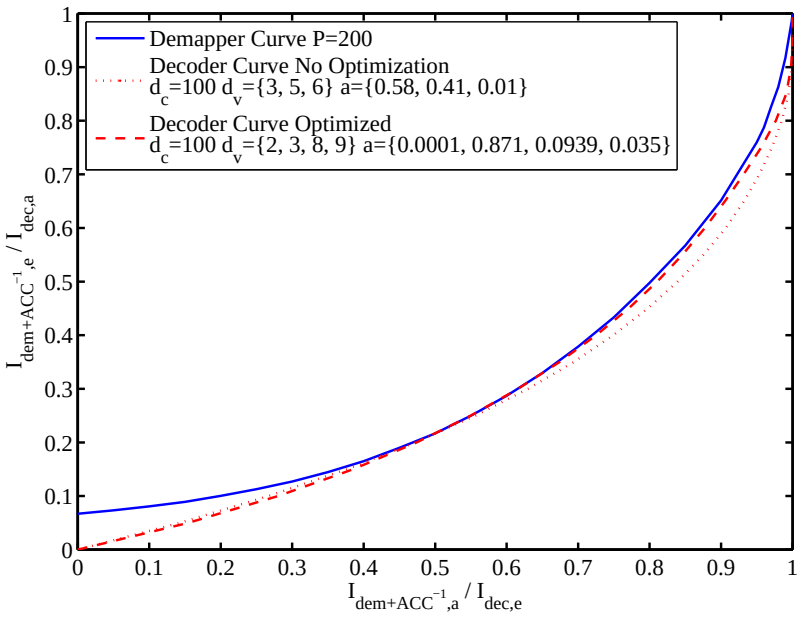

Figure 5.7: EXIT Chart using Partial Accumulator at SNR = 3.1 dB

Chapter 6

EXIT-constraint Binary Switching Algorithm and Unbalanced Labeling

The labeling pattern, used in the SPCCIRC-BICM-ID-EM technique, is, designed to achieve left most of the demapper EXIT curve as larger as possible. However, as presented in the previous chapter, partial accumulator lifts the right-most point of the demapper EXIT curve up to the $(1.0, 1.0)$ MI point. Therefore, the labelling pattern has to be redesigned aiming at better matching between the demapper and the decoder EXIT curves. In this chapter, a new technique to achieve optimal labelling pattern is described.

6.1 Cost Calculation and Binary Switching Algorithm

Labelling pattern shown in Fig. 6.1 for SPCCIRC-BICM-ID-EM is obtained by using Binary Swtiching Algorithm (BSA) where labelling cost function defined in this section used for optimization. In [14], labelling cost refers to pairwise error probability for the AWGN channel with full *a priori* information. Assuming that average pairwise probability full *a priori* of $l_{map} - 1$ bits is assumed to be known except the bit to be detected, average pairwise error probability $Z_{l_{map}-1}$ between the two symbols, originally transmitted symbol s and to other symbols $\hat{s}$, is given by,

$$Z_{l_{map}-1} = \frac{1}{l_{map} 2^{l_{map}}} \sum_{v=1}^{l_{map}} \sum_{s|s_v=0} \sum_{\hat{s}|\hat{s_v}=1} exp(-SNR|\mu(s_v) - \mu(\hat{s}_v)|^2)) \tag{6.1}$$

where function $\mu(\cdot)$ returns the constellation point of a symbol $s_v$and v denotes the vth bit of a symbol. This average pairwise probability given by (6.1) is used as a cost

function, which can be further decomposed as sum of the cost functions for each fixed symbol s^h,
given $Z_{l_{map}-1} = \sum_{h=0}^{2^{l_{map}}-1} Z^h_{l_{map}-1}$, where,

$$Z^h_{l_{map}-1} = \frac{1}{l_{map}2^{l_{map}-1}} \sum_{v=1}^{l_{map}} \sum_{s^h|s^h_v=0} \sum_{\hat{s^h}|\hat{s^h_v}=1} exp(-SNR|\mu(s^h_v) - \mu(\hat{s^h_v})|^2)) \tag{6.2}$$

and $h = 0, 1, ..., 2^{l_{map}} - 1$. The BSA is shown in **Algorithm 2**. Problem with

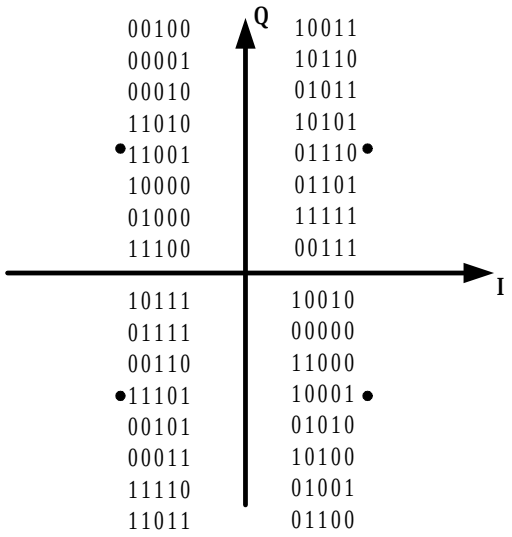

Figure 6.1: 4-QAM Extended Mapping

Algorithm 2 Binary Switching Algorithm (BSA)

repeat
  Initialization: generate labelling pattern randomly.
  Select the symbol s_{high} which has the highest cost $Z^h_{l_{map}-1}$.
  Find the symbol s_{low} which can achieve maximum reduction the total cost $Z_{l_{map}-1}$ by swapping the positions of S_{high} and S_{low}.
  if s_{low} exists. **then**
    Swap s_{high} and s_{low}.
    Update $Z_{l_{map}-1}$ according to the new labelling pattern.
  else
    Set the symbol with the second highest cost as s_{high}.
  end if
until There is no pair of symbols to switch

this approach is, however, that the cost is calculated only assuming there is a full a priori information and thus, $Z_{l_{map}-1}$ only affect the right most point of the demapper EXIT curve. Therefore, demapper EXIT curve using the BSA does not consider the matching between the demapper and decoder EXIT curve. This approach is reasonable only when the objective is to make the right-most point of the demapper curve to reach as close to the $(1.0, 1.0)$ MI point as possible. However, since thesis has proposed the use of PA which already makes it possible that the demapper EXIT curve reaches a point close enough to the $(1.0, 1.0)$ MI point. In the next section, a novel algorithm, EBSA, is introduced to obtain a labelling pattern aiming at better matching between the two curves.

6.2 EXIT constraint Binary Switching Algorithm

Given l_{map}, number of known bits l_{ap}, which satisfies

$$l_{ap} = 0, 1, ..., l_{map} - 1. \tag{6.3}$$

For the labelling cost $Z_{l_{ap}}$ with the l_{ap} known bits from a priori information, $Z_{l_{ap}}$ can be expressed as,

$$Z_{l_{ap}} = \frac{1}{l_{map} 2^{l_{map}-1} 2^{l_{map}-l_{ap}-1}} \sum_{v=1}^{l_{map}} \sum_{s|s_v=0} \sum_{\hat{s}|\hat{s}_v=1} exp(-SNR|\mu(s_v) - \mu(\hat{s}_v)|^2)). \tag{6.4}$$

Furthermore, as $Z_{l_{ap}}$ can be decomposed into symbol wise cost $Z^h_{l_{ap}}$, as,

$$Z_{l_{ap}} = \sum_{h=0}^{2^{l_{map}}-1} Z^h_{l_{ap}} \tag{6.5}$$

with

$$Z^h_{l_{ap}} = \frac{1}{l_{map} 2^{l_{map}-1} 2^{l_{map}-l_{ap}-1}} \sum_{v=1}^{l_{map}} \sum_{s^h|s^h_v=0} \sum_{\hat{s}^h|\hat{s}^h_v=1} exp(-SNR|\mu(s^h_v) - \mu(\hat{s}^h_v)|^2)). \tag{6.6}$$

Labelling cost matrix for l_{map} is defined in as $l_{map} \times 2^{l_{map}}$ matrix as,

$$Z = \begin{bmatrix} Z^0_0 & Z^0_1 & \cdots & Z^0_{l_{map}-2} & Z^0_{l_{map}-1} \\ Z^1_0 & Z^1_1 & \cdots & Z^1_{l_{map}-2} & Z^1_{l_{map}-1} \\ & & \vdots & & \\ Z^{2^{l_{map}}-1}_0 & Z^{2^{l_{map}}-1}_1 & \cdots & Z^{2^{l_{map}}-1}_{l_{map}-2} & Z^{2^{l_{map}}-1}_{l_{map}-1} \end{bmatrix} \tag{6.7}$$

Note the $2^{l_{map}} - 1th$ low of the matrix Z corresponds to the case where all bits in the label are zero, i.e,

$$\begin{aligned} Z^{l_{map}-1} &= \begin{bmatrix} Z_0^{2^{l_{map}}-1} & Z_1^{2^{l_{map}}-1} & \cdots & Z_{l_{map}-2}^{2^{l_{map}}-2} & Z_{l_{map}-1}^{2^{l_{map}}-1} \end{bmatrix} \\ &= \begin{bmatrix} 0 & 0 & \cdots & 0 & 0 \end{bmatrix} \end{aligned} \tag{6.8}$$

Now given l_{ap}, $l_{ap} = 0, 1, \cdots, 2^{l_{map}} - 1$, the total cost $\hat{\mathbb{Z}}$ for each l_{ap} is calculated by simply summing the column vector of Z as,

$$\begin{aligned} \hat{\mathbb{Z}} &= \begin{bmatrix} Z_0 & Z_1 & \cdots & Z_{l_{map}-2} & Z_{l_{map}-1} \end{bmatrix} \\ &= \begin{bmatrix} 1 & 1 & \cdots & 1 & 1 \end{bmatrix} \begin{bmatrix} Z_0^0 & Z_1^0 & \cdots & Z_{l_{map}-2}^0 & Z_{l_{map}-1}^0 \\ Z_0^1 & Z_1^1 & \cdots & Z_{l_{map}-2}^1 & Z_{l_{map}-1}^1 \\ & & \vdots & & \\ Z_0^{2^{l_{map}}-1} & Z_1^{2^{l_{map}}-1} & \cdots & Z_{l_{map}-2}^{2^{l_{map}}-1} & Z_{l_{map}-1}^{2^{l_{map}}-1} \end{bmatrix} \\ &= \begin{bmatrix} \sum_{h=0}^{2^{l_{map}}-1} Z_0^h & \sum_{h=0}^{2^{l_{map}}-1} Z_1^h & \cdots & \sum_{h=0}^{2^{l_{map}}-1} Z_{l_{map}-1}^h \end{bmatrix} \end{aligned} \tag{6.9}$$

These costs affect the shape of the demapper EXIT curve. Fig. 6.2 shows an intuitive example for $l_{map} = 5$. Now weighting vector $\boldsymbol{\lambda}$ is introduced to take into account that which cost is important from the viewpoint of the matching between the two EXIT curves. The weighted cost $\bar{Z}$ (scaler) can be expressed as following using $\boldsymbol{\lambda}$, as

$$\bar{Z} = \hat{\mathbb{Z}}\boldsymbol{\lambda} = \hat{\mathbb{Z}} \begin{bmatrix} \lambda_0 & \lambda_1 & \cdots & \lambda_{l_{map}-2} & \lambda_{l_{map}-1} \end{bmatrix}^t. \tag{6.10}$$

Using λ, symbol wise weighted cost vector $\bar{\mathbb{Z}}$ can also be calculated as

$$\bar{\mathbb{Z}} = Z\boldsymbol{\lambda} = \begin{bmatrix} \bar{Z}^0 & \bar{Z}^1 & \cdots & \bar{Z}^{2^{l_{map}}-1} \end{bmatrix}^t \tag{6.11}$$

with

$$\bar{Z} = \sum_{i=0}^{2^{l_{map}}-1} \bar{Z}^i \tag{6.12}$$

Using these costs values, this thesis introduces a EXIT-constraint Binary Switching Algorithm (EBSA), which is described in **Algorithm 3**. For the gap checking, vertical distances between the two curves are considered instead of horizontal gap 6.3. Note that the labelling pattern used in the LP-based optimization with partial accumulator are obtained by lowering the the cost of $Z_{l_{map}-1}$ (at right-most MI point corresponding to with full a priori information) as much as possible. As a consequence, other costs $Z_0, \cdots, Z_{l_{map}-2}$ are ignored.

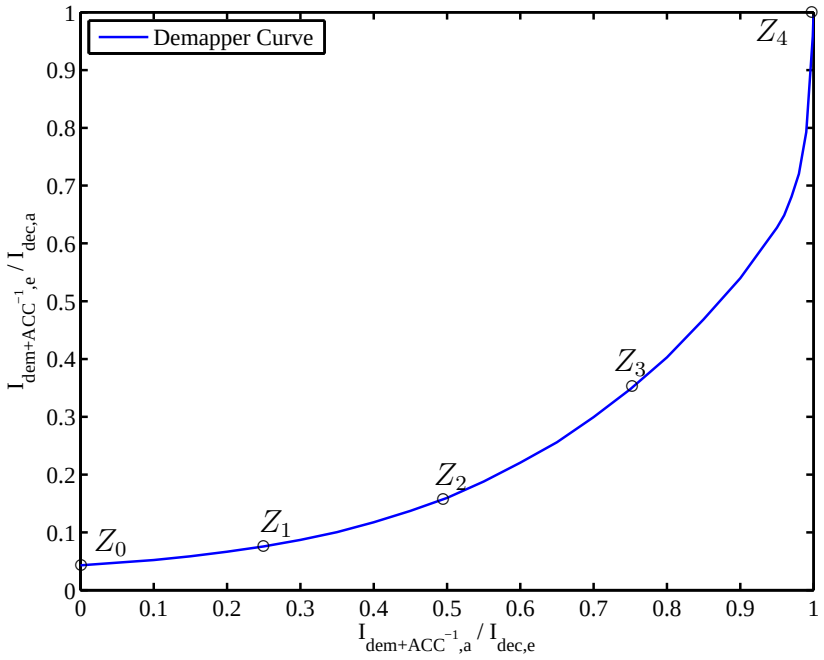

Figure 6.2: Points Affected by Labelling Costs

Algorithm 3 EXIT-constraint Binary Switching Algorithm (EBSA)

$\lambda = \begin{bmatrix}\lambda_0 & \lambda_1 & \cdots & \lambda_{l_{map}-2} & \lambda_{l_{map}-1}\end{bmatrix} = \begin{bmatrix}0 & 0 & \cdots & 0 & 1\end{bmatrix}$

repeat

  for $i = 1$ **to** N_{max}[1] **do**

    Randomly generate labeling pattern.

    Conduct BSA with $Z_{l_{map}-1} = \bar{Z}$ and $Z^h_{l_{map}-1} = \bar{Z}^h$.

  end for

  Select the labeling pattern with minimum $\hat{Z}$ from the N_{max} trial of BSA.

  Draw demapper EXIT curve and LP-aided decoder EXIT curve, and check the gap between the two curves.

  if The gap in the range of $MI(Z_{l_{ap}} \pm \Delta Z_{l_{ap}})$[2]around Z_{ap} is larger than desired value $\epsilon'_{l_{ap}}$ **then**

    $\lambda_{ap} = \lambda_{ap} - 1$

  end if

until Gap between the demapper and decoder EXIT curve becomes smaller than the threshold for each MI points tested.

[2]Ref.[14] shows that $N_{max} = 100$ is enough.

[3]where $\Delta = 1/(l_{map} - 1)$.

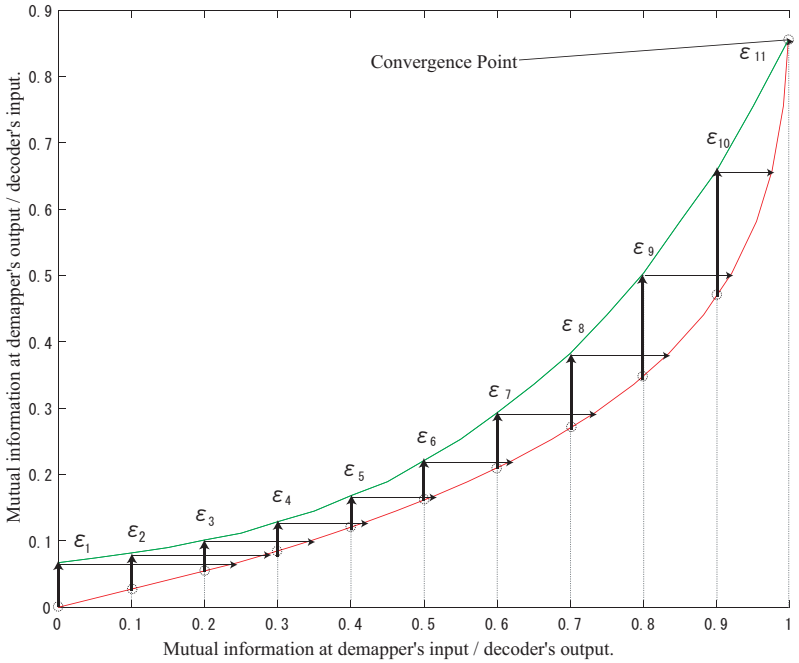

Figure 6.3: Gap Checking in EBSA

6.3 EXIT Analysis

By performing EBSA, the labelling pattern shown in Fig. 6.4 is obtained. Fig. 6.5 shows the EXIT chart of demapper and decoder EXIT curve using the labelling pattern shown in Fig. 6.4 and degree allocation obtained from EBSA. The demapper and the decoder EXIT curves are closely matched. However, the demapper curve starts from the $(0, 0)$ MI point and hence two EXIT curves intersect at the $(0, 0)$ MI point. Since two EXIT curves cross at the $(0, 0)$ MI point, trajectory stacks at the $(0, 0)$ MI point and hence LLR exchange can not be initiated. Therefore, a technique to slightly lift up the left-most of the demapper EXIT curve is required. In the next section, a technique to make this possible is introduced.

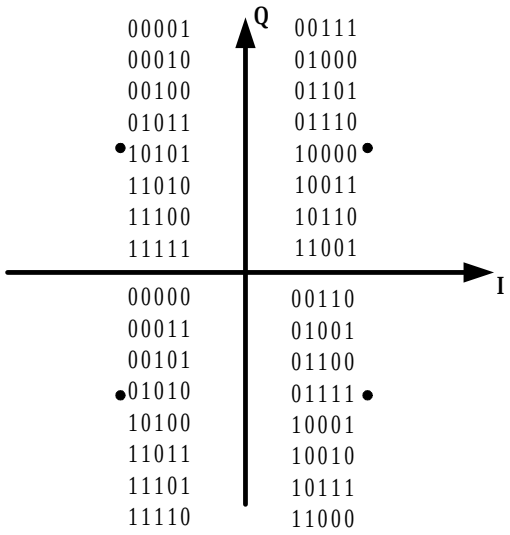

Figure 6.4: Obtained Labelling Pattern from EBSA

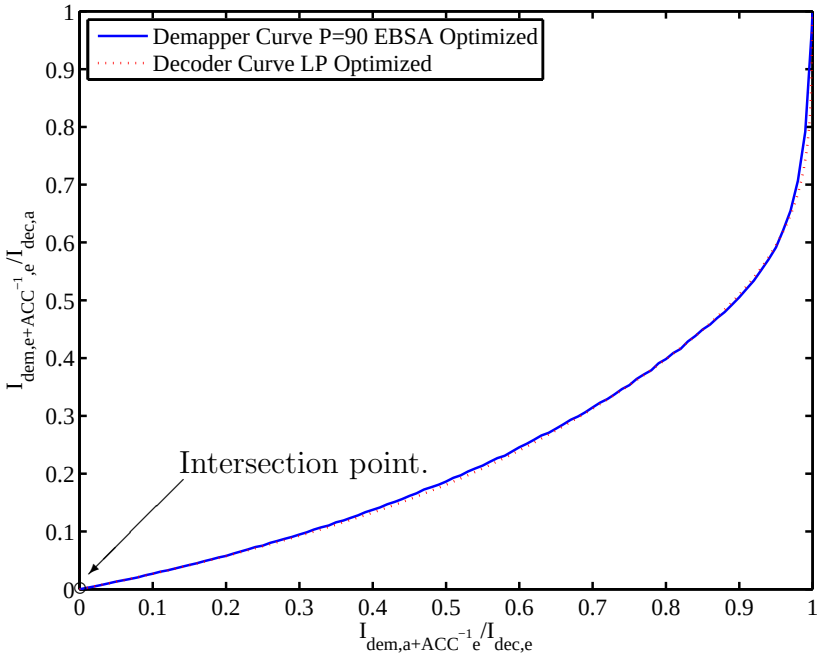

Figure 6.5: EXIT Chart of Balanced Labelling and EBSA at SNR = 1.0 dB

6.4 Unbalanced Labeling

As mentioned in section 3.5, number of constellation points significantly affect the area below the demapper EXIT curve. On the contrary, the labelling pattern less significantly affects the area, while it affects the shape of the curve. Using this principle, this thesis proposes a random generation of unbalanced labelling pattern instead of balanced labelling pattern. An example of the unbalanced labelling pattern is depicted on Fig. 6.6. From the cost calculation viewpoint, moving a label from one constellation point to another point does not change the cost drastically. As a result, unbalanced labelling slightly decreases a cost with no a priori information. This is because from (6.8), cost of symbol with all the bits being ('11....11') is always zero. Now, this technique can also be explained from the viewpoint of the MI in the EXIT chart. Per-bit entropy $H_{balanced}$ of balanced labelling pattern for 2^M-QAM without any a priori information can be expressed as,

$$H_{balanced} = -\frac{1}{M}\sum_{t=1}^{2^M} P_r(t)\log P_r(t) = 1 \tag{6.13}$$

where t denotes the constellation point, and $P_r(t) = 1/2^M$. In the same way, per-bit entropy $H_{unballanced}$ of unbalanced labelling pattern can be derived as,

$$H_{unbalanced} = -\frac{1}{M}\sum_{t=1}^{2^M} P_r(t)\log P_r(t) \tag{6.14}$$

where $P_r(t)$ is the appearance probability of the constellation point t. For example, $P_r(t) = [8/32\ 8/32\ 7/32\ 9/32]$ for the unbalanced 4-QAM labelling pattern shown in Fig. 6.6. In this case, $H_{unbalanced} = 0.99715$. From (6.13) and (6.14), it is found that using unbalanced labelling, uncertainty of demapping is reduced by $1 - 0.99715 = 0.0185$(bits) compared to that with balanced mapping. Consequently, the reliability of demapper's extrinsic LLR with no a priori information is increased, which is consistent with (3.9), where if the conditional entropy $H(B|L)$ decreases, MI $I(B;L)$ increases.

6.5 EXIT Chart Analysis

Fig. 6.7 shows the EXIT chart where EBSA and unbalanced labelling is applied to SPCCIRC-BICM-ID-EM. Close matching between the demapper and decoder EXIT curve can be observed from the starting point to the end. Moreover, now the demaper curve starts from $(0, 0.0029)$ and thereby, iteration can be initiated, and the trajectory reaches a point close enough to the $(1.0, 1.0)$ MI point.

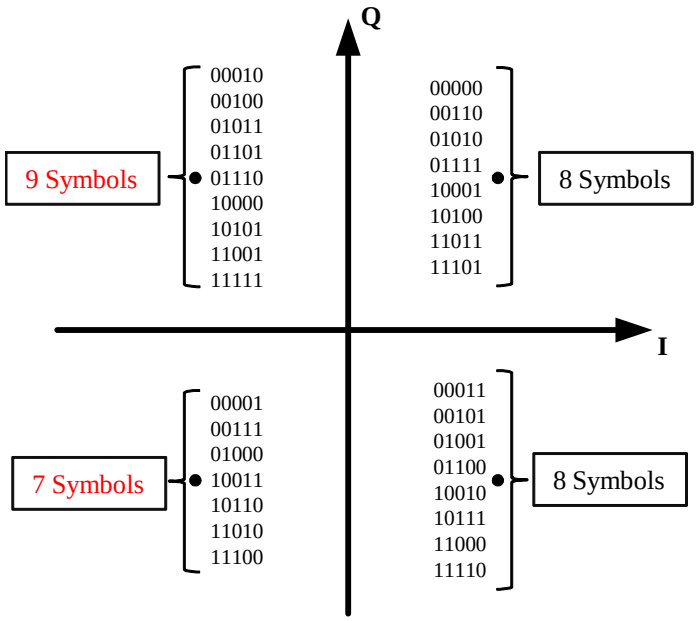

Figure 6.6: Unbalanced 4-QAM Extended Mapping.

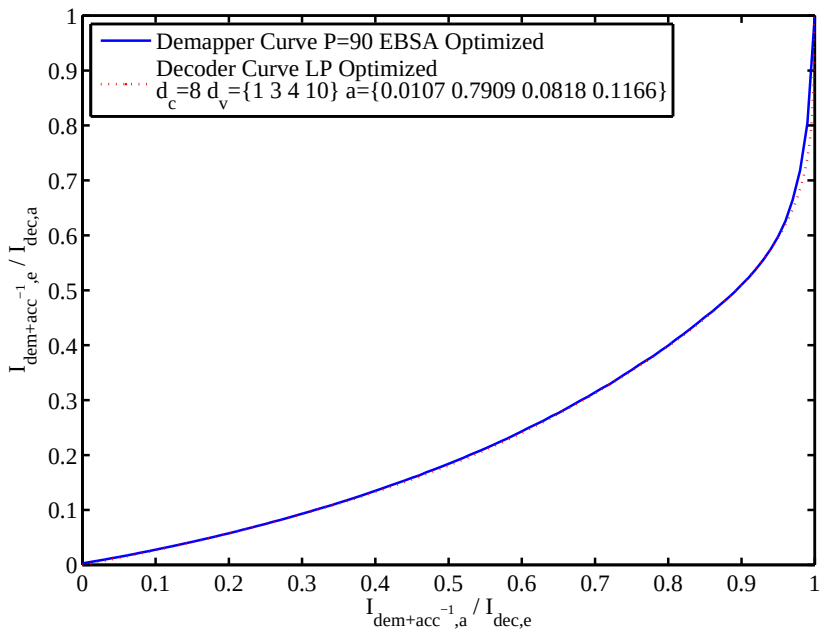

Figure 6.7: EXIT Chart of Unbalanced Labelling and EBSA at SNR = 1.0 dB

Chapter 7

Performance Evaluation

Several new techniques have been proposed in this thesis with the aim of achieving near-Shannon limit performance with SPCCIRC-BICM-ID. In this chapter, results of BER simulations conducted to evaluate BER and convergence performance of the proposed systems are shown.

7.1 Irregular Degree Allocation Optimization using LP

Fig. 7.1 shows non-optimized and optimized BER versus SNR curves. It is found that when the degree distribution is optimized at SNR = 0.9 dB, the spectrum efficiency is 0.95 bits/symbol, which is 0.05 bits/symol higher the the empirically designed case [5][11]. The 0.9 dB threashold SNR , where the turbo cliff happens, for 0.95bits/symbol is 1.3 dB away from the Shannon limit.

7.2 Partial Accumulator

Fig. 7.2 shows the BER of SPCCIRC-BICM-ID-EM, of which partial accumulator. The BER curves with and without LP optimization are shown, where the degree distribution empirically obtained in [5] were used for non-optimized design. It is found that when the degree distribution is optimized, the spectrum efficiency is 1.076 bits/symbol, which is 0.1602 bits/symol higher than the empirically designed case. The threshold SNR for 1.076 bits/symbol if 1.4 dB, as observed in Fig. 7.2, is only 0.95 dB away from the Shannon limit. Furthermore, it is found that, by using the proposed partial accumulater, BER floor can be completely eliminated.

7.3 EBSA and Unbalanced Labelling

Fig. 7.3 shows the BER of SPCCIRC-BICM-ID-EM of which EBSA and unbalanced labelling is introduced. The best result among those tested achieves the threshold SNR of 0.54 dB away from the Shannon limit, for which parameters are shown in the box below the BER figure. It should be noted that approximately 300 iterations were needed when SNR is around the threshold.

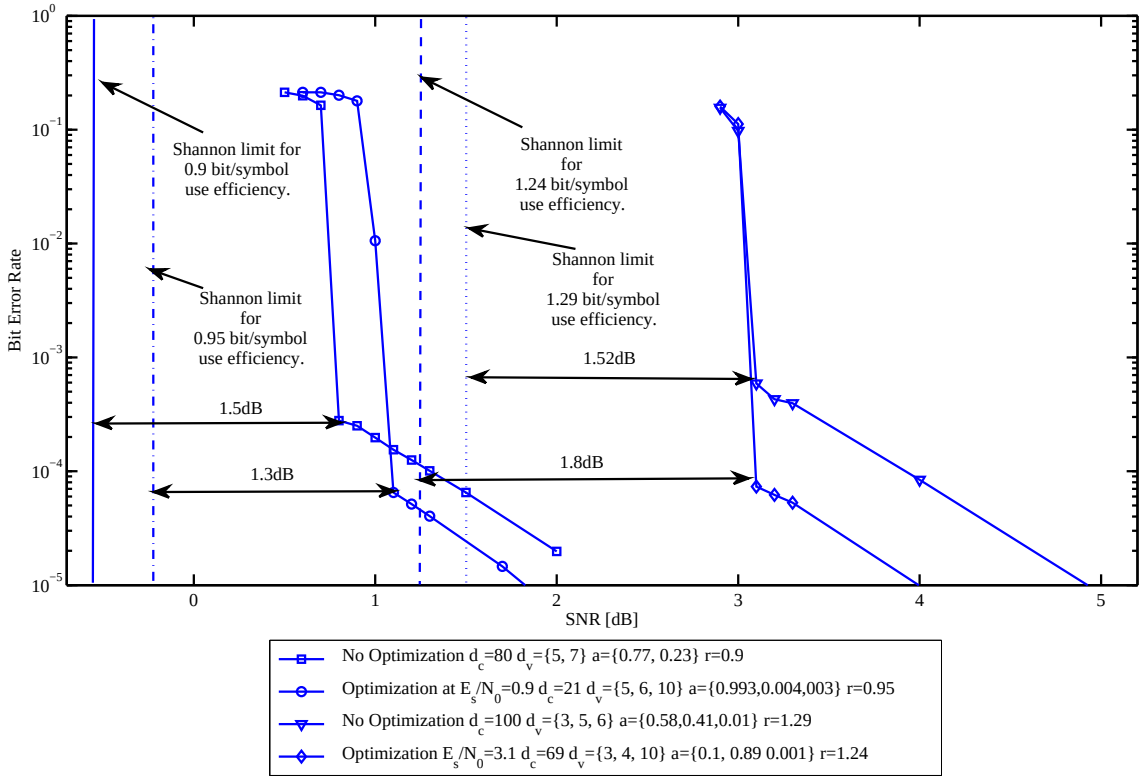

Figure 7.1: BER Chart: Optimization using LP

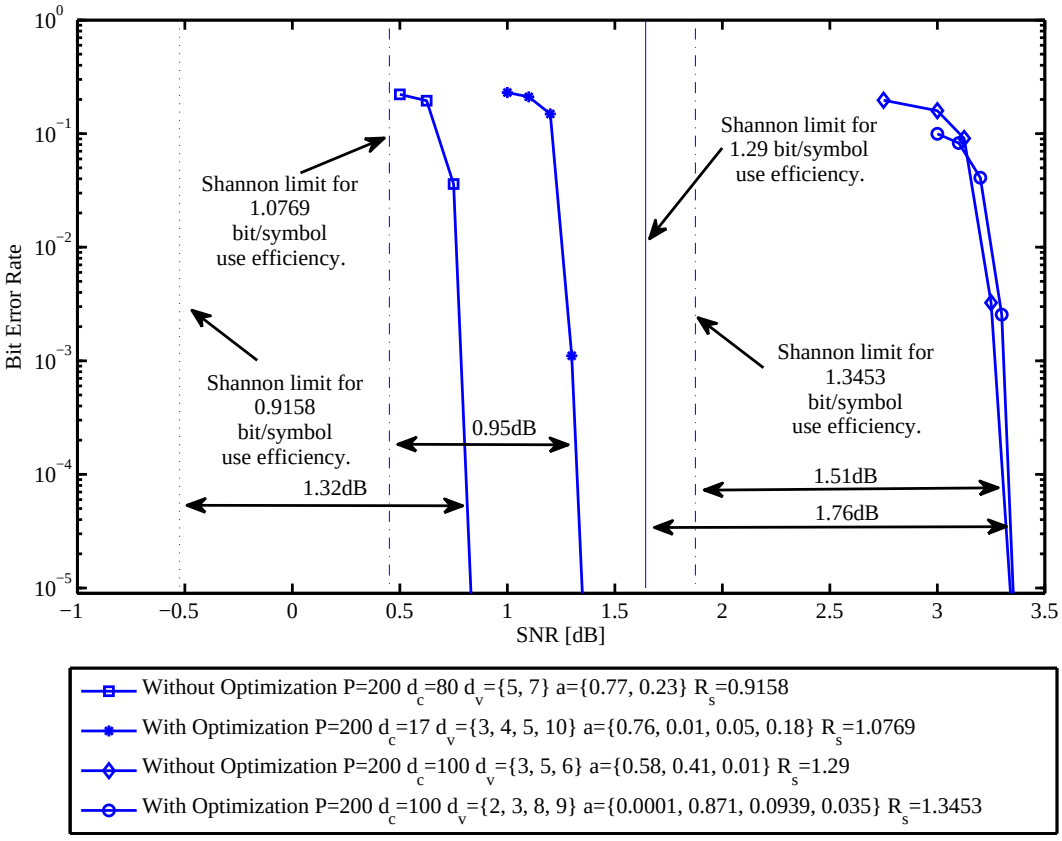

Figure 7.2: BER Chart: Partial Accumulator

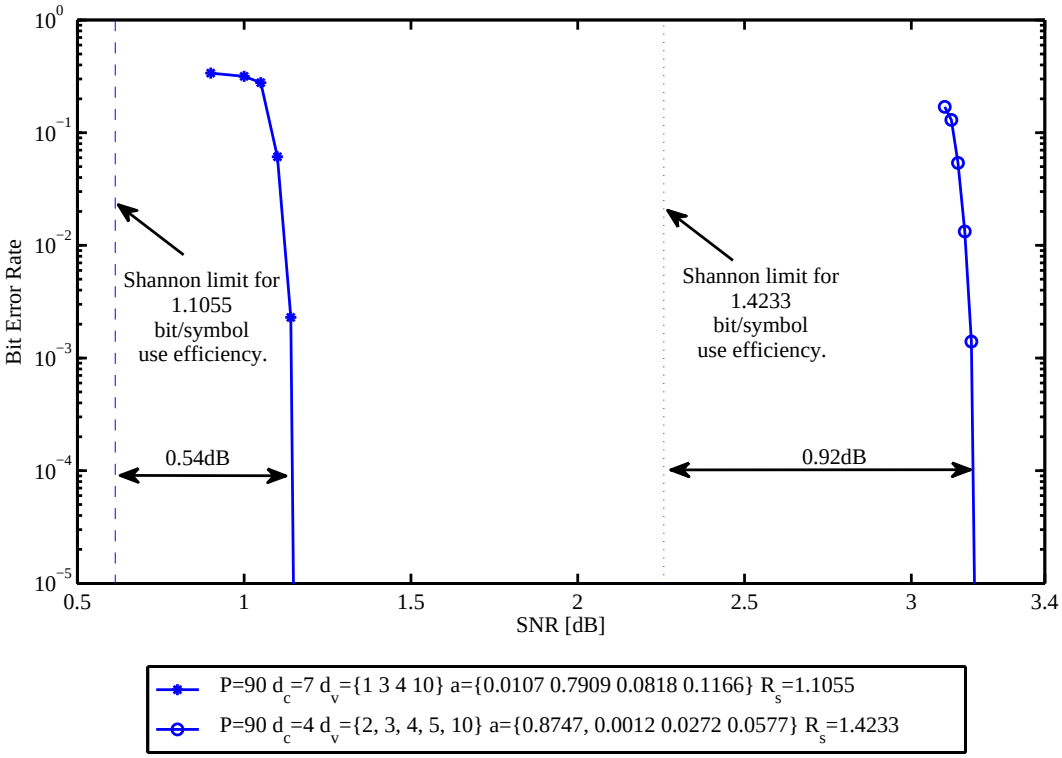

Figure 7.3: BER Chart: EBSA and Unbalanced Labelling

Chapter 8

Conclusions

This thesis discussed the problem of SPCCIRC-BICM-ID-EM through step-by-step analysis of the EXIT chart. Based on the EXIT analysis, this thesis proposed four major techniques with the aim of achieving near Shannon-limit performance for the SPCCIRC-BICM-ID-EM techniques.

Chapter 2 introduced fundamentals of wireless communications followed by the explanation of the BICM-ID technique. Furthermore, SPCCIRC-BICM-ID is introduced and its BER performance was presented.

Chapter 3 introduced the of EXIT chart for performance analysis as well as for the design of iterative systems. In addition, performance analysis of SPCCIRC-BICM-ID-EM using EXIT chart was provided in this chapter.

Chapter 4 introduced a technique to systematically derive a degree allocation using LP. EXIT analysis was also provided in Chapter 3 with the LP technique, higher spectrum efficiency and lower BER can be expected. However, there still is a problem that error floor can not be eliminated with the LP optimization. This is because the demapper and decoder EXIT curves intersect at a point (X, Y), where $X \approx 1.0$ but $Y < 1.0$.

Chapter 5 proposed a combined use of partial accumulator and SPCCIRC-BICM-ID. This technique is introduced to lift up the right-most point of the demapper EXIT curve so that it intersect with the decoder curve at a point close enough to $(1.0, 1.0)$ MI point. EXIT chart analysis confirms that the use of partial accumulator is of significant importance in the proposed system. Furthermore, only except the left-most potion, smooth matching between the demapper and decoder curve is achieved by using the partial accumulator and LP aided optimization.

Chapter 6 pointed out that with the partial accumulator, labelling pattern must be redesigned, aiming at better matching of the two EXIT curves. This is because the labelling pattern in chapters 4 and 5 was designed so that the right-most point of the demapper EXIT curve approaches the $(1.0, 1.0)$ MI point. However, the combined use of partial accumulator lifts the demapper EXIT curve up to a point close enough to the $(1.0, 1.0)$ MI point. Chapter 6, novel technique, EBSA and unbalanced labelling

were introduced to obtain the optimal labelling pattern considering the matching between the two EXIT curves.

Chapter 7 provided the performance evaluation results of the proposed techniques using BER simulations. By the use of EBSA, most significant result can be obtained: a turbo cliff happing at SNR = 0.54 dB away from the Shannon limit. The results confirm that with the use of EBSA and unbalanced labelling, near optimal performance of SPCCIRC-BICM-ID-EM can be achieved. In addition, it should be noted that the complexity of the SPCCIRC-BICM-ID-EM technique is at the same level as a turbo code with only memory-2 convolutional constituency codes. If the same performance in terms of the threshold SNR as the proposed SPCCIRC-BICM-ID-EM system is required with the turbo code, memory-4 convolutional constituency codes have to be used, of which the decoding complexity is approximately 4 times the system proposed in this thesis.

Acknowledgements

The research work for this thesis was conducted while I was serving as a master-course researcher in the Matsumoto Lab, School of Information Science, Japan Advanced Institute of Science and Technology from June 2009 till March 2011. This place is great environment for research work. In addition, I was lucky to meet nice and interesting people during my research work.

First of all, I am heartily thankful to my supervisor, Professor Tad Matsumoto. My research work started with almost no knowledge about information and coding theory based wireless communications. I had a great guidance and advices from him, including fundamental elements. Today, I am writing this thesis with successful results delivered in a short period of time. It goes without saying that I could not be able to reach this point without his passionate support. Again, I would like to thank Professor Tad Matsumoto from my bottom of heart.

Special thanks to Assistant Professor Khoirul Anwar's invaluable support. His advices always hit the point and it was inevitable to proceed my research work.

My gratitude also goes to my lab mates. Their support were always grateful and they have stimulated my spirit towards research work.

The financial support provided by Hitachi Kokusai Electric Inc. is highly acknowledged. Practical advices and suggestion they gave me from industry viewpoint where always helpful and I would especially like to thank Mr.Kobayashi for this point.

I would like to thank my close friends for all their help and support during my research period; Akihiro Ikeda, Hiroko Mitarai, Masashi Suguro, Miwa Kanazawa, Shuichi Sowa and Takeshi Kojima.

My warmest appreciation goes to my parents Isaburo and Ritzuko, my elder sister Monami and elder brother Tomohisa for their caring they gave me throughout my life.

Bibliography

[1] C. E. Shannon, "A mathematical theory of communication," *Bell Systems Technical Journal*, vol. 27, pp. 379–423,623–656, 1948.

[2] X. Li and J. Ritcey, "Bit-interleaved coded modulation with iterative decoding," *Communications Letters, IEEE*, vol. 1, no. 6, pp. 169 –171, Nov. 1997.

[3] S. ten Brink, "Convergence behavior of iteratively decoded parallel concatenated codes," *Communications, IEEE Transactions on*, vol. 49, no. 10, pp. 1727 –1737, Oct. 2001.

[4] J. Hagenauer, "The exit chart - introduction to extrinsic information transfer in iterative processing," in *Proc. 12th Europ. Signal Proc. Conf (EUSIPCO)*, 2004, pp. 1541–1548.

[5] D. Zhao, A. Dauch, and T. Matsumoto, "BICM-ID Using Extended Mapping and Repetition Code with Irregular Node Degree Allocation," in *Vehicular Technology Conference, 2009. VTC Spring 2009. IEEE 69th*, Apr. 2009, pp. 1–5.

[6] D. Huffman, "A method for the construction of minimum-redundancy codes," *Proceedings of the IRE*, vol. 40, no. 9, pp. 1098 –1101, 1952.

[7] C. Berrou and A. Glavieux, "Near optimum error correcting coding and decoding: turbo-codes," *Communications, IEEE Transactions on*, vol. 44, no. 10, pp. 1261 –1271, Oct. 1996.

[8] M. Tuchler, R. Koetter, and A. Singer, "Turbo equalization: principles and new results," *Communications, IEEE Transactions on*, vol. 50, no. 5, pp. 754 –767, May 2002.

[9] L. Hanzo, *Turbo Coding, Turbo Equalisation and Space-Time Coding for Transmission over Fading Channels*. New York, NY, USA: John Wiley & Sons, Inc., 2002.

[10] P. Henkel, "Extended mappings for bit-interleaved coded modulation," in *Personal, Indoor and Mobile Radio Communications, 2006 IEEE 17th International Symposium on*, 2006, pp. 1 –4.

[11] D. Zhao, A. Dauch, and T. Matsumoto, "Modulation doping for repetition coded BICM-ID with irregular degree allocation," in *ITG Wireless Smart Antenna*, Berlin, Feb. 2009.

[12] S. Pfletschinger and F. Sanzi, "Error floor removal for bit-interleaved coded modulation with iterative detection," *Wireless Communications, IEEE Transactions on*, vol. 5, no. 11, pp. 3174 –3181, 2006.

[13] S. ten Brink, "Rate one-half code for approaching the shannon limit by 0.1 db," *Electronics Letters*, vol. 36, no. 15, pp. 1293 –1294, Jul. 2000.

[14] F. Schreckenbach, N. Gortz, J. Hagenauer, and G. Bauch, "Optimized symbol mappings for bit-interleaved coded modulation with iterative decoding," in *Global Telecommunications Conference, 2003. GLOBECOM '03. IEEE*, vol. 6, 2003, pp. 3316 – 3320 vol.6.

Achievements

- K. Fukawa, D. Zhao, A. Tolli, and T. Matsumoto "Irregular Repetition and Single Parity Check Coded BICM-ID using Extended Mapping" *IEEE Communications and Networking in China (ChinaCom) 2010*, Beijing Aug. 25, 2010
- K. Fukawa, K. Anwar, A. Tolli, and T. Matsumoto "Design of Simple Shannon Limit Approaching BICM-ID" *IEICE National Conference 2011-spring*, Tokyo Mar. 15, 2011

.

List of Notations

$\bar{b}$ delayed bits, page 36

$\bar{Z}$ weighted cost of labelling pattern, page 45

$\boldsymbol{\lambda}$ weighting vector, page 45

ϵ acceptable gap between the demapper and the decoder EXIT curves, page 30

$\gamma(s, s')$ branch metric for BCJR, page 38

$\hat{b}$ partial accumulator output bits, page 36

$\hat{\mathbb{Z}}$ total cost of labelling pattern having l_{ap} bits are known, page 45

log natural logarithm to base 2, page 7

$\mu(\cdot)$ constellation point of the argument, page 42

ν_n zeron mean Gaussian distribution, page 23

σ_n^2 variance of AWGN, page 12

a node degree allocation, page 11

A_{dec} Area under the decoder EXIT curve, page 23

A_{dem} Area under the demapper EXIT curve, page 23

B bandwidth of the system, page 7

B source, page 20

b source information, page 4

b' channel coded bits, page 36

C channel capacity, page 7

d_c check node degree, page 11

d_v node degree, page 11

$E[\cdot]$ expectation of the variable, page 20

$erfc(\cdot)$ complementary error function, page 24

f_c Center frequency, page 5

h index for symbol, page 43

$H(\cdot)$ entropy of the variable, page 20

$H_{balanced}$ per-bit entropy of balanced labelling pattern, page 49

$H_{unbalanced}$ per-bit entropy of unbalanced labelling pattern, page 49

i index for irregular node degrees and node degree allocations, page 12

$I(\cdot;\cdot)$ mutual information, page 20

$I_{dec,a}$ *a priori* MI input for decoder, page 22

$I_{dec,e}$ *extrinsic* MI output from decoder, page 23

$I_{dem,a}$ *a priori* MI input for demapper, page 22

$I_{dem,e}$ *extrinsic* MI output from demapper, page 22

$J(\cdot)$ J-function, page 22

K source information sequence length, page 5

K' channel coded sequence length, page 5

L LLRs, page 9

l_{ap} number of know bits from the *a priori* information, page 44

l_{ap} number of known bits, page 44

$L_{cnd,e}$ *extrinsic* LLR output from check node, page 17

$L_{dec,a}$ *a priori* LLR input for decoder, page 17

$L_{dec,e}$ *extrinsic* LLR input from decoder, page 17

$L_{dem,a}$ *a priori* LLR input from demapper, page 17

$L_{dem,e}$ *extrinsic* LLR output from demapper, page 16

l_{map} bits per symbol, page 12

log_{10} natural logarithm to base 10, page 7

M number of bits per symbol, page 6

m symbol timing index, page 12

n zero mean complex AWGN component, page 12

P index of replaced bit in partial accumulator , page 36

$Pr(\cdot)$ probability of the variable, page 4

R code rate, page 5

$R_{S,SPCCIRC}$ total spectrum efficiency of SPCC and IRC, page 12

$R_{SPCCIRC}$ total code rate of SPCC and IRC, page 12

S set of symbol labels, page 16

s symbol, page 16

t constellation point, page 49

x transmitted modulated signal, page 12

y received signal, page 12

Z cost matrix, page 44

$Z_{l_{ap}}$ cost of labelling pattern having l_{ap} bits are known, page 44

$Z_{l_{map}-1}$ cost of labelling pattern with full *a priori information*, page 42

$Z^{h}_{l_{map}-1}$ cost of symbol h with full *a priori* information, page 43

Index